Numerical Analysis of Work Roll Cooling in Hot Rolling Process

Thesis submitted in partial fulfillment
of the Requirements for the degree of

Master of Technology

in

Mechanical Engineering

Specialization: Thermal Engineering

by

Shaibu V B

Roll no: 210me3247

Department of Mechanical Engineering
National Institute of Technology Rourkela
Rourkela, Odisha, 769 008, India
June 2012

Numerical Analysis of Work Roll Cooling in Hot Rolling Process

Thesis submitted in partial fulfillment
of the Requirements for the degree of

Master of Technology
in
Mechanical Engineering
Specialization: Thermal Engineering

by

Shaibu V B
Roll no: 210ME3247

Under the guidance of
Prof. S K SAHOO

Department of Mechanical Engineering
National Institute of Technology Rourkela
Rourkela, Odisha, 769 008, India
June 2012

Dedicated to My Parents

Department of Mechanical Engineering
National Institute of Technology
Rourkela-769 008, Odisha, India.

Certificate

This is to certify that the work in the thesis entitled **Numerical Analysis of Work Roll Cooling in Hot Rolling Process** by **Shaibu V B** is a record of an original research work carried out by him during 2011 - 2012 under my supervision and guidance in partial fulfillment of the requirements for the award of the degree of Master of Technology with the specialization of **Thermal Engineering** in the department of **Mechanical Engineering, National Institute of Technology Rourkela**. Neither this thesis nor any part of it has been submitted for any degree or academic award elsewhere.

Place: NIT Rourkela
Date: 04 June 2012

Prof. S K SAHOO
Department of Mechanical Engineering
NIT Rourkela, Odisha

Acknowledgments

Completion of this project and thesis would not have been possible without the help of many people, to whom I am very thankful. First of all, I would like to express my sincere gratitude to my supervisor, **Prof. S K Sahoo**. His constant motivation, guidance and support helped me a great deal to achieve this feat.

I would like to thank Prof. R. K. Sahoo, Prof. A. K. Satapathy, Prof. Alok Satapathy and Prof. S Murugan for guiding and inspiring me in many ways. I am also thankful to other faculty and staff of Mechanical Engineering department for their support.

I would like to thank all my friends, especially Baburaj M and Shiba Narayan Sahu for their help during the course of this work. I would like to mention the names of Chithra R, Lokesh K, Denny K Philip Rahul R and Aswani Kumar for their endless support for the betterment of the work.

I am deeply indebted to my parents who always believed in me and gave all their support for all the choices that I have made.

Finally, I humbly bow my head with utmost gratitude before the God Almighty who always showed me a path to go and without whom I could not have done any of these.

Shaibu V B

Roll no: 210ME3247

shaibu.vb@gmail.com

Contents

Abstract

In hot rolling process the work rolls is subjected to succeeding heating and cooling cycles with the net effect of heat influx. This nature of heating might cause damage at the same time as shape imperfections in the rolled slabs. Therefore it is the essential to know how the temperature of the work rolls increases. This particular phenomenon has been modelled and simulated with the help of ANSYS 13 Software. Based on the three dimensional heat equations and temperature fields of a roll were investigated using finite element method (FEM). For the estimation of thermal field on the work roll, mathematical modelling of moving heat sources approach is executed. The differences in the surface temperature of the roll during hot rolling process were illustrated. The effect of orientations of the water jets, heat transfer coefficient at roll surface and hot strip entry temperature also been deliberated by this model, and their effect on roll temperature has been analysed. The change of angle of jet has shown that the effect of heat transfer coefficient is reduced. The computational dynamics of fluid flow with heat transfer variation and its characteristic are analytically modelled using the Finite volume Method (FVM). The method is illustrated to determine the heat transfer coefficient distribution of an array of liquid water spray type which are used to cool the rolls on a steel strip rolling mill. Heat transfer data are obtainable for an array of 60^0 cone sprays including the effect of controlling off array members. The average heat transfer coefficient of the jet impingement is $5000 W/m^2K$. All the simulations are carried out for both steady state and transient changes in roll. By the effect of optimized cone spray water jet cooling, the surface temperature of the work roll will be decreased from 723^0C to an average temperature of 40^0C.

List of Figures

List of Abbreviations

CFD	Computational Fluid Dynamic
CVC	Continuous Variable Crown
FDM	Finite Difference Method
FEM	Finite Element Method
FVM	Finite Volume Method
HSM	Hot Strip Mill
HT	Heat Transfer
HTC	Heat Transfer Coefficient
Nu	Nusselt Number
Pr	Prandtl Number
Re	Reynolds Number
RPM	Revolutions Per Minute

1 Introduction

Rolling is one of the processes of metal working in which changes the dimension and shape of metal of metal stoke or work piece are produced with the application of pressure by contact with cylindrical rolls. Metal rolling process are classified into two different category as per the working temperature is hot rolling process and cold rolling process. If that process is doing with above re-crystallization temperature is called hot rolling process. In hot rolling process steel slabs are heated from a reheating furnace before being processed. The heated steel slabs from the furnace are rolled to attain its desired dimension through different steps. In the first step it rolled through roughing mill and finished in finishing mill in second step. Sometimes, more than one rough mill is used, if its size reduction rate is high. The reduced slabs are then cooled on a run out table to a prefixed cooling temperature. (Figure 1.1) shown below will get a brief description about the process flow of a hot strip mill.

The most important part of this entire process is rolling in the finishing mill.

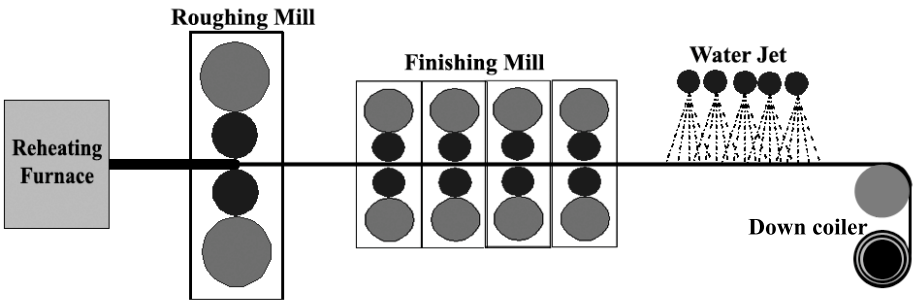

Figure 1.1: Process Flow diagram of Hot Rolling Process

Four or more finishing stands are contains in the finishing mill section. Each stand consists of two work rolls and two back rolls simultaneously reduce the thickness and temperature of the strip. During this rolling process an incredible amount of heat transfer will happened from the slab to the work rolls, it deteriorates the roll surface. For getting better work roll life and arrest this deterioration heat transfer to the roll surface, will provide forced water cooling on rolls. An additional advantage of this water cooling is the reduction in the oxide formation on roll surface.

From the past years research works have carried out a wide range of investigation in rolling process to develop the models for the prediction of roll temperature profile and to minimize the thermal fatigue during rolling. Research works have mainly focused on the thermal profile across the boundary layer of the work roll surface. They proposed, to investigate the work roll, have been used both one dimensional and two dimensional models. Axis-symmetric finite element and finite difference methods have also been used to find the transient temperature profile of the roll with the effect of water spray variables. United analysis of slab temperature and roll temperature leads that the roll temperature variation are not the same at all stands. Resent work with this analysis of work roll and temperature profile in hot and cold rolling has been mentioned in the literature.

A high quality strip is required to satisfy not only its mechanical and physical criterias, but it should also be produced to the required geometrical or dimensional tolerances. One of the main defects to producing the shape is the inappropriateness of the incoming profile of the strip with respect to the geometry of pass. The crowning of the work rolls is one variable along with many other variables related to the pass geometry. The control of crowning or profile is most important to avoid such defects. Estimation of the total heat transfer and temperature profile of work roll is included in this work and depended factors of heat transfer and variation of temperature in heating and cooling process also described. Combined effect of conduction, convection and radiation is considered for the prediction of heat transfer effect in heating and cooling cycles, especially jet impingement heat

transfer in forced convection cooling cycle. The awareness of the temperature distribution in the work roll is dominant, due to the requirement for exact estimation of the thermal crown for preserving required profile and flatness. The behavior of the roll bite region and the water cooled region of the roll is analyzed for a limited number of revolutions.

1.1 History of Rolling

According to Wagoner and Chenot, The rolling process can be defined as a constant process of plastic deformation for long parts of stable cross section, in which a reduction of the cross-sectional area is achieved by compression between two or more rotating work rolls. In cold rolling process the solid metal is deformed at room temperature. But it can be somewhat higher than ambient temperature due to heat dissipation by plastic work. And in hot rolling process the temperature is high than ambient temperature. It is somewhat more than half of the absolute melting temperature. Another significant difference is made based on the geometric considerations, which are flat rolling, slab rolling and sheet rolling. If the thickness of strip or sheet is very small, of the order of millimeters or less, that rolling process is called as flat rolling and this is also the condition for sheet rolling or strip rolling. If the strip or metal thickness is of the order of 0.1 m and any in between condition, that is done with slab rolling. Shape rolling is used for the construction of more complex work pieces by using proper work roll geometries. Figure 1.2 represents the general method for flat rolling and two cases of geometries in a vertical cross section by a plane parallel to the rolling direction.

For hot rolling or cold rolling of any geometry, the preferred reduction of cross-sectional area is too bigger to be practical in one pass. The last deformation is gradually applied by using various stands so that different number of pairs of cylinders successively deforms the same part as shown in Figure 1.3. There are thus related forces between two successive stands, which persuade tension in plane loads, either in the direction of rolling or in the reverse direction. In Figure 1.3, the smaller work rolls are in contact with the strip or sheet and produce successive reduction of thickness. The small diameters limit the width of the deformation

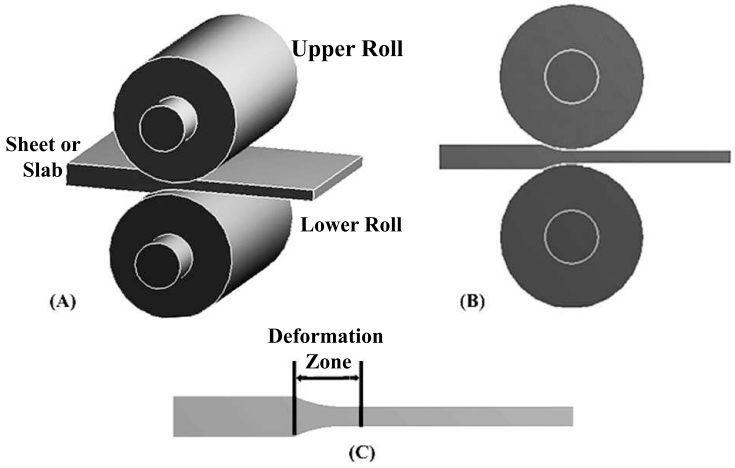

Figure 1.2: Flat rolling: (a) general, (b) cross section for slab rolling,(c) cross section for sheet rolling

region and thus the roll separating force. The bigger diameter work rolls are designed to prevent unnecessary bending of the work roll.

It has long been thought that rolling, which accounts for about 90 percent of all metals produced by metal working processes, was first developed in the late 1500s. However, it was none other than the great Leonardo da Vinci, who, in the section of his note books dedicated to the study of mechanisms and machines, first described an exact and fully functional design of a rolling mill dedicated to the flat rolling process.

As reported by Cianchi, Leonardo da Vinci describes in his notebooks that these two machines were intended for producing sheets of tin by making the metal pass between the principal rollers. In the sketch on the top there is however,

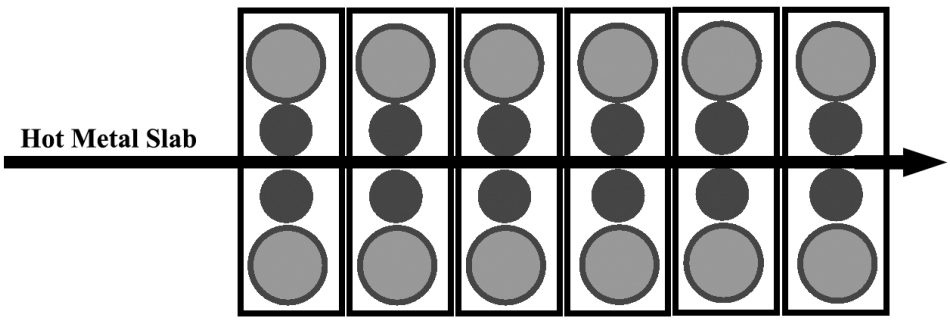

Figure 1.3: Schematic of a five-stand rolling mill

an important addition, two smaller rollers, which keep up the pressure on the principal ones so that the sheet produced is homogeneously smooth. This method is still employed.

In the 1500s and 1600s very primitive mills were used to work roll sheets of gold, silver, tin, and even for making coins. The use of work rolls in an iron works was a German development of the 16th century. Belgium and England both started to use work rolls about the same time, and so these three countries are considered as the birthplace of rolling. By 1682 Great Britain had become the leading nation in the rolling industry and the first records of hot rolling appear, with large rolling mills for the hot rolling of ferrous materials near Newcastle, England. From that point and during the early part of the eighteenth century, rolling mills expanded to the continent.

During the early part of the 18th century, Christopher Polhem from Sweden, designed the first mill with 4 work rolls, with the backup work rolls driven, in a very similar manner to how the modern Lauth mill works. In 1728 a patent for a mill to work roll hammered bars was issued to John Payne in England. Also, in 1766, another Englishman, John Purnell received a patent for grooved work rolls with coupling boxes and nut pinions for turning the work rolls in unison. It is in this same period, that the general appearance of these hot mills began to change to the modern form. For example, the cast housing and the single screw on each side of the mill became a standard by William Playfield in 1782. Roberts describes how the eighteenth century also saw the advent of the tandem mill in which the metal is rolled in successive stands. Richard Ford patented the first true tandem mill of which there is record in England in 1766, for the hot rolling of wire rods. A later patent issued in 1798, refers to a tandem mill for the rolling of hot plates and sheets and in the same year, John Hazeldine added mechanical guides to a rod mill.

In the beginning of the 19th century, the industrial revolution in England was gathering momentum, creating an unprecedented demand for iron and steel. Accordingly, rolling mill developments were numerous and important. John Biken-

shaw started the first rail rolling mill in 1820 producing wrought iron rails in lengths of 15 to 18 feet. In 1831 the first T rail was rolled in England and the first I beams were rolled by Zores in Paris in1849. Three high mills were also introduced about the middle of the century. A British patent for such a mill, designed for rolling heavy sections, was granted in 1853 to R. Roden. In this mill, the middle work roll was driven and fixed in the housing while the upper and lower work rolls were adjustable in position. On the same mill, a steam-operated lifting table raised and lowered the material to be rolled. In mid century, the first reversing plate mill was put into operation at the Park gate Works in England, and in 1854 it was used to work roll the plates for the Great Eastern steam ship. In 1848, R.M. Daelen of Lendersdorf, Germany, who also built the first mill of this type about seven years later, invented the universal mill. The first mill constructed on the continuous principle of rolling iron or steel was patented to Charles White of Wales.

Roberts also writes: "a British patent issued in 1862 to J.T. Newton of Wales, described a predecessor to the modern cluster mill, in as much as it used small work rolls backed up by others of large diameter. The work rolls were driven but the pressure was applied by the large backup work rolls, a principle utilized in both the hot and cold mills of today". The four-high mill with its work rolls in the same vertical plane was introduced in 1872 by Bleckley of England; Tandem rolling of hot steel took an upsurge around 1890, and in 1892, a semi-continuous hot strip mill, with a mechanically geared two-high tandem finishing train, was built at Bohemia. As reported by Roberts, the first record of tandem cold rolling of steel strip goes back to about 1904, when the West Leechburg Steel Company installed and operated a 2-high 4-stand tandem mill, each stand being driven by a separate, adjustable speed dc motor. Reel tandem mill operation, with tension between stands, and a tension reel was developed around 1915, on mills in Pittsburgh, Pennsylvania. Finally, in the late 80s and in the beginning of the 1990s, the rolling industry began to take advantage of the development of the CNC and CAD/CAM technology, particularly applied to the design and manufacture of work rolls for

hot-rolled steel special section profiles.

1.2 Objective of the Present Work

The review with the existing literature two dimensional finite element methods (FEM) and finite difference method (FDM) have been used for find the temperature field and thermal stress field of work roll. In the present work, three dimensional temperature distribution of work roll during rolling process is simulated using FEM and Finite volume method (FVM). It is found that coupled three dimensional simulations of thermal profiles and CFD analysis of water jet cooling is too much complicated in nature. CFD analysis of jet impingement heat transfer is simulated in ANSYS 13 CFX solver and ANSYS 13 Transient Thermal modular is used for the analysis of conduction, convection and radiation part of the roller in this analysis. An analytical model predict the variation of work roll temperature at the end of whole operation and periodic repetition will leads the exact definition of heat transfer effect.

1.3 Methodology and present conditions

In the hot rolling mill, the slabs from the furnace are rolled into strips by reducing their thickness from 210mm to a value ranging from 1.6mm to 12mm, while the range of the width of the strip is from 600 mm to 1540mm. The slabs, coming from the Furnace, are heated and saturated in a walking beam type reheating furnace so as to attain the required temperature of 1250 deg C for the deformation of the slab to obtain the appropriate thickness. The hot slab from the furnace is cleaned with high-pressure jets to remove the layer of oxide from the slabs and which they are feed in to the roughing mill. There are several passes in the four-high reversing roughing mill in the specific hot strip mill, after which the temperature of the slab is reduced to about 1050 deg C, and the thickness is reduced to 24mm. The rolls are housed in the 4 high finishing mills with two work rolls and two backup rolls to support the work rolls. After rough milling process deformation is attained from tandem finishing mill with a finish rolling temperature of 870 deg C to 900 deg C depending on the grades. Centrifugally cast high-chrome work rolls are used in

the finishing mill to attain the required metallurgical properties at different coiling temperature. The strip from the finishing mill is cooled with high pressure water jets in the run out table and coiled finally in the down coiler. Estimation and control of thermal profiles of work roll in finishing mill are simulated in this work with different variables, which are roll diameter, roll rotation speed and width. The roll diameter will be varying from 850 mm to 600 mm and the widths of roll are 600 mm, 500mm. the roll rotation speed also varied from 200 rpm to 60rpm.

2 Literature Review

2.1 Work roll analysis

Martha P. Guerrero, Carlos R. Flores, Antonino Perez and Rafael Colas[1] developed a heat transfer model for hot rolling work rolls in 1999. Three models have been implemented to determine the transient heat flow. Finite-difference method was used for the generation of two models and another one generated by integrating the heat flow to the roll. A fourth model was steady-state based model generated by the integration of the heat flow. It is concluded that each model has its own value, and that all of them have to be used when a complete analysis of the rolling conditions is required. Another model for developing the temperature and stress fields in work rolls during hot rolling was employed by F.D. Fischer, W.E. Schreiner, E.A. Werner and C.G. Sund [2]in 2004. They mainly focused on the application of the solution for the temperature field of a moving heat source as a logical and programmable expression allows approximate the temperature field close to the surface layer of a work roll. They considered the friction and surface contact factors for these calculations. Also basic expressions for the stress field close to the surface layer are accessible. Heat is transferred by a moving heat source of density. Several previous contributions do not reflect on the fact of a moving heat source, and their domino effects thus are at least doubtful.

C. H. HUANG and T. M. JU [3] in 1994 developed a model for the analysis of surface thermal characteristics of the working roll in hot rolling process. They employed the two-dimensional inverse analysis [4-6] of conjugate gradient method. It was a minimization method, applied to calculate the surface thermal performance

of a roll which was employed in steel rolling mills with water jet cooling. From their analysis, it can be found that no previous information is required for the functional forms of time wise and space wise deviation of the surface layer temperature and heat flux. The transient temperature footage within the roll is modified from the presented experimental data and serves as the simulated data for the inverse analysis. The results explain that the evaluation of surface temperature and heat flux becomes inferior when the temperature measurements are taken too far away from the surface, due to a thin thermal layer. Sudipta Sikdar and Shylu John[7] focused a model for finding the work roll temperature in a hot strip mill by the effect of water jet orientation and other controlling Parameters. Water jet cooling is used to dissipate the thermal energy from the body of a roll during its repeated movement in the finishing stands of a hot strip mill. The temperature distribution of the roll in each stand of finishing stage of a hot strip mill has been numerically analyzed by a mathematical model. The effect of jet orientations, heat transfer coefficient at roll jet interface region and slab entry temperature has been evaluated by this model, and their effect on work roll temperature has been simulated. The change of jet angle has found that the effect is negligible.

Y.T. Azene , R. Roy , D. Farrugia, C. Onisa , J. Mehnen and H. Trautmann[8] developed a optimization model for Work roll cooling system design. This model presents a structure to optimize the design of work roll according to the cooling performance. This model develops from a set of finite element analyses of the work roll cooling. A design of testing technique is employed to identify the FEA runs. The research also recognizes sources of suspicions in the design process. A strong evolutionary multipurpose estimation technique is implemented to the design and optimization in constrained problems with real life hesitation. This method handles uncertainties associated both with fitness functions and design variables. M raudensky, J Horsky and M Pohanka [9] developed an optimization model of roll cooling. In this model a laboratory experimental set up was developed to allow full scale measurement on work roll cooling to be carried out. The full scale tests use a full relationship of rows of nozzle as in the plant environment

or prepared by a designer. This method allows the design to be optimized or to evaluate old and new solutions. The test provides a profile of cooling intensity at the roll surface. The second step of the optimization process is the practice of a numerical model for calculation of temperature and work roll crown in a hot rolling region. A typical industrial rolling schedule is employed to test the efficiency of cooling. A typical purpose of the experimental and numerical method is in intensification of rolling, in improvements of cooling, and in design work. Example of the results and general recommendations for cooling are incorporated in this model.

Mohamed Hamraoui [10] proposed a model for finding out the thermal behavior of rollers during the rolling process. It was a numerical study developed to establish the two-dimensional temperature profile in the work roll of a rolling mill. The considered hot rolling mill consists of two hollow cylinders receiving heat in contact with the work piece and cooled by convection on its internal and external surfaces. This method is carried out in steady state regime and is focused in the thermal behavior of a single cylinder of the rolling mill. A hollow circular cylinder is considered, receiving a heat flux on a portion of its outer surface and being cooled on the remains. The internal surface layer of the circular cylinder is also cooled. The model is validated by consideration with an analytical solution and the thermal behavior as a function of the angular velocity of the cylinder and the conditions of heat exchange with the environment is analyzed. Important conclusions are deduced from this model that can be of a large utility for the sizing of this type of rollers and the analysis of their mechanical behavior.Mohammad Abbaspour and Ahmad Saboonchi [11] focused on the thermal expansion control of work roll in hot strip mill. work roll thermal crown plays an significant role in controlling strip contour and flatness of the strips. They done with a faultless and convenient cooling system which also takes care of the roll against damage persuaded by fire cracking. In this model a computer simulation based finite difference method is employed under transient condition to estimate the temperature and thermal expansion in the roll. This model had the capability of accepting dif-

ferent boundary condition in axial and circumferential direction for varies cooling configurations such as using varies types and numbers of nozzles and positioning in different direction. The results of this simulation are compared and confirmed with an actual hot rolling program data for which the temperature of a roll was measured at Mobarakeh Steel Complex. They developed a computer based model for work roll cooling system on finite difference method to estimate the work roll temperature and associated thermal expansion.

Pao Tung Hsu , Yue Tzu Yang and Chao-Kuang Chen [12] established a three dimensional (3d) Inverse model for estimate the surface thermal behavior of the work Roll in hot rolling Process. A three-dimensional inverse analysis employs a different perspective to calculate the thermal behavior of the work roll in rolling process in this analysis. This analysis is based on the temperature variations taken inside the roll at different locations. Finite difference methods are employed to discrete the problem at first stage and then a linear inverse model is created to recognize the boundary conditions. The linear least squares method is assumed to find the solution. The advantages of this analysis are that no prior information is required concerning the functional form of the unknown variables and no initial guess required to use and the numbers of iterations for estimation process. From this analysis, it can be found that only few measuring points are enough to approximate the boundary conditions when measurement fault are neglected. When measurement mistakes are considered, more measuring points are required in order to increase the correspondence of the projected results to exact solutions. S. Serajzadeh [13] employed a model for find out temperature distribution in the hot rolling of steels by the effects of rolling parameters. Temperature distribution of work rolls in the hot rolling of steel slabs was analyzed by solving heat conduction equation with transient boundary conditions. The Raylieght Ritz and the finite element methods (FEM) were implemented to solve the governing equation. In his model, the thermal relationship between rolling metal and rolls was taken into account with the effects of varies parameters such as rolling speed, interface heat transfer coefficient, and strip initial temperature were considered in the cal-

culations. His result was show that the rolling speed and interface heat transfer coefficient are important factors.

Two dimensional FEM analyses have been carried out to calculate the temperature profile and the effect of different factors together with the thermal relationships to the roll and the metal strip, and the rolling speed [14]. Current work with the coupled analysis of work roll and slab temperature in cold rolling, Arif and khan [15-16] has been established in his work. Understanding of thermal crown due to the change of work roll gap heat transfer coefficient has mentioned in the model of Ye, X and Samarasekera [17]. A FEM model has been used to determine the two-dimensional temperature profiles of the strip and the roll [18]. Presently, an analytical model [19] expects the increase of roll temperature at the end of an entire operation cycle is found from the curve of the thermal response for a roll. Rapid reduction of the work roll surface temperature is shown there. By means of a hybrid, analytic and numerical model, the thermal response of the rolls used for hot rolling of steel slab has been explained [20]. The model demonstrate flexible behavior to contain the changes in the thermo physical properties of the rolls or for changes in equipped parameters such as temperature profile or the rolling pace or length of slabs. Another research work [21] investigated the possibility of lowering work roll surface temperature by the coordinated arrangement of use of work roll gap lubrication and ant peeling system with the conventional cooling. Average surface temperature has been established to be reduced along with the diminution of the oxide formation due to ant peeling system.

2.2 Jet impingement heat transfer analysis

Stevens and Webb [23] carried out early studies regarding liquid jet impingement with round nozzles. It considered an axis symmetric, single phase liquid jet impinging on a flat consistently heated surface for investigates the effects of nozzle to plate spacing, Reynolds number and jet diameter. Garimella and Rice [24] calculated the local heat transfer experimentally from a small heat source to a usually impinging, axis-symmetric and submerged liquid (FC-77) jet from a round nozzle

for a range of Reynolds number of 4,000-23,000 and nozzle to heat source spacing ratios of 1 to 14 and concluded that secondary peaks in the local heat transfer coefficient resulted from increasing nozzle diameters for a given Reynolds number. Heat transfer from a vertical heated surface to an obliquely impinging circular free-surface jet of transformer oil for various Reynolds number (235-1,746) with jet angles from 45 to 90 has been performed by Gomi and Webb [26]. They found that the maximum heat transfer coefficient decreases with increasing jet inclination. Lee et al. [27] experimental study concluded that the stagnation point Nusselt number increases with increasing surface curvature by using convex surface with low curvature using liquid crystals to measure the local surface temperature at Reynolds numbers ranging from 11,000-50,000. Kornblum and Goldstein [28] explored the flow of circular jets impinging on convex and concave surfaces for relatively small jet to semicylindrical diameter ratios ranging from 0.0197-0.0394 via flow visualization technique. To obtain information on the stagnation and local Nusselt numbers, Lee et al. [29] employed an apparatus consisting of various components (heat exchanger, flow meter, and air blower) to target a convex hemispherical surface for Re=11,000-87,000 at different dimensionless nozzle-to-surface distance and at constant hemisphereto-nozzle diameter ratio. Tong [30] statistically studied convective heat transfer of a circular liquid jet impinging onto a substrate using the volume-of-fluid method to track the free surface of the jet.

Cornaro et al. [31-32] visualized fluid flow using a smoke-wire technique on concave and convex surfaces to examine the effects of curvature, nozzle to surface distance, and Reynolds number. He also showed the effect of increasing Reynolds number on the local Nusselt number for different types of curvature. In [33], Fleischer et al. used a smoke-wire flow visualization technique to investigate the behavior of a round jet impinging on a convex surface. The effects of Reynolds number, jet to surface distance, and relative curvature were considered. Baonga et al. [34] experimentally studied the hydrodynamic and thermal characteristics of a free round liquid jet impinging into a heated disk for nozzle to plate spacing of 3-12 times nozzle diameter and for Reynolds number of 600-9,000.

One of the early investigations on jet impingement on a flat plate was conducted by Inada et al. [35] who studied laminar flow between a plane surface and a two-dimensional water jet with constant heat flux using the Runge-Kutta method to obtain solutions for the boundary layer momentum and energy equations. Related analytical solution to the momentum equation was developed by Carper [36]. Liu and Lienhard [37] methodically and experimentally investigated convective heat transfer to an impinging liquid jet from a heated flat surface kept at a uniform heat flux. An experiment to investigate single phase heat transfer from a smooth simulated chip to a two-dimensional jet of dielectric liquid FC-72 delivered from a very thin rectangular slot jet into a 5 channel confined between the chip surface and nozzle plate has been done by Wadsworth and Mudawar [38]. Gau and Chung [39] reported heat transfer for air jet impingement on semicylindrical curved surfaces at low and high Reynolds numbers (6,000-35,000) by varying slot widths to surface diameter ratios (0.022-0.125) using smoke particles as means to visualize the air flow. Stevens and Webb [40] experimentally characterized the flow structure under an impinging liquid jet hitting a flat surface.

3 Mathematical modelling

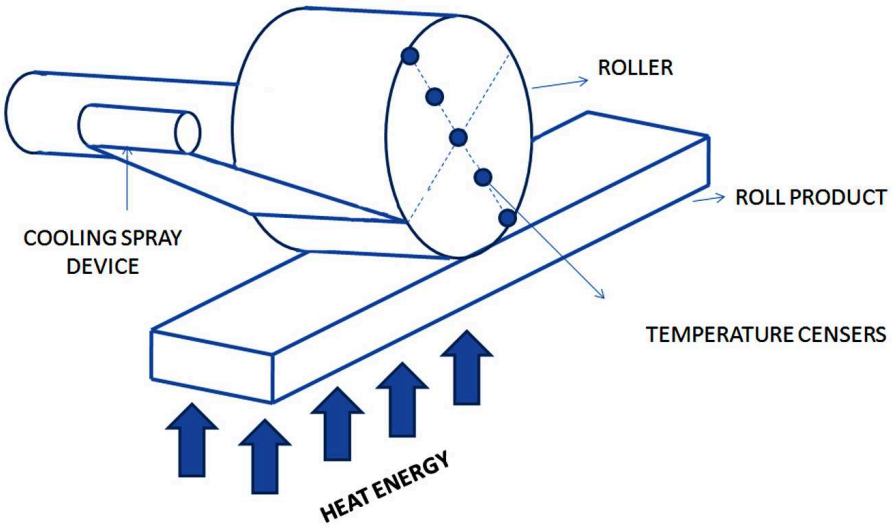

Figure 3.1: Simple Line Diagram of Hot Rolling Process

This chapter presents varies heat transfer models of work roll. Numerous analytical solutions are obtained for calculating the average thermodynamic quantities at the work roll bite region and different interfaces. The simple line diagram of hot rolling process model is demonstrated in Figure 3.1. Various geometric configurations almost similar to real processing is considered for the analysis with appropriate assumptions. For creating models of the work roll, can be assumes as different angular sectors. Each angular sector created by the division with its sole

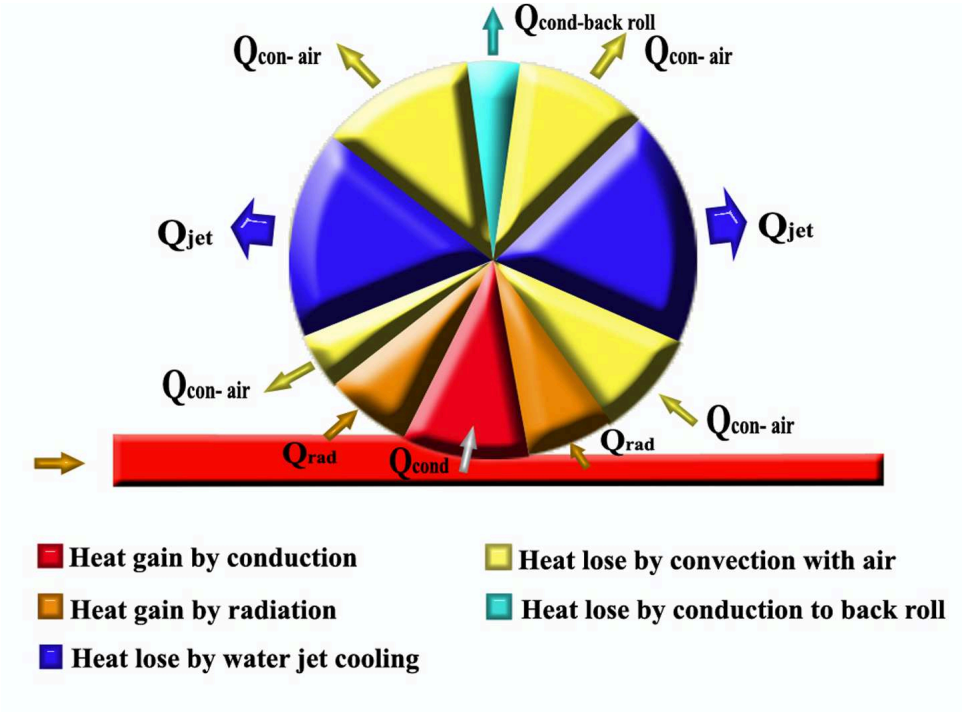

Figure 3.2: Heat Flow Distribution of Different Angular Sectors of a Work Roll

heat-transfer conditions. Figure 3.2 explains the exact heat transfer positions of work roll. It is considered that work roll heat transfer occur only by conduction, convection and radiation. The net heat transfer was separated in to two groups, which is heating and cooling.

The heating arise by conduction and radiation from strip and the cooling or heat removal occurs by convection to the air and forced convective heat transfer effect of jet impingement on the roll surface. Conduction to back roll also happen in some cases. According to the first low of thermodynamic, the total heat transfer of the system to be conservative. So the net heat transfer to the system by the effect heating must be equal to the net heat transfer from the system by the effect of cooling. So the mathematical model analysis is done on the basis of these heat transfer division. Heating part and cooling part are to be calculating separately. Three dimensional temperature distribution of work roll during rolling process was simulated using FEM and Finite volume method (FVM) in this work. This thesis is discussing about the all condition of heat transfer itself. Mathematical modelling is categorized by

- Heating model
  - Conduction model
  - Radiation model
- Cooling model
  - Conduction model
  - Jet impingement model
  - Convection model
- Combined model

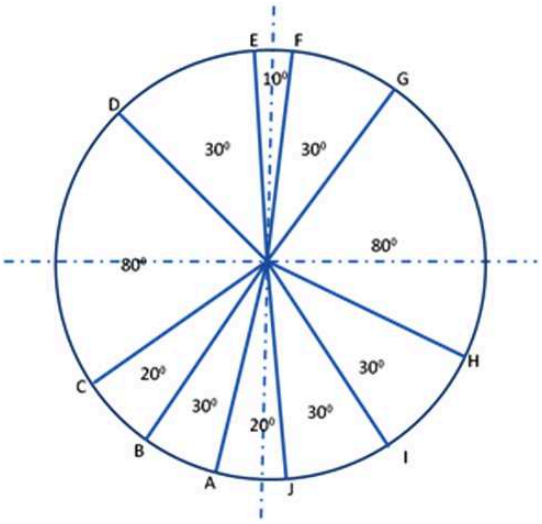

Figure 3.3: Boundary conditions of different zones

A-B	radiation heat gain to the roll from hot strip (radiation zone 1)
B-C	convective heat lose from roll to air (convection zone 1)
C-D	water jet cooling by the effect of jet impingement (impingement zone 1)
D-E	convective heat loses from roll to air surface (convection zone 2)
E-F	heat lose due to conduction from roll to back roll (conduction zone 2)
F-G	convective heat lose from roll to air (convection zone 3)
G-H	water jet cooling by the effect of jet impingement (impingement zone 2)
H-I	convective heat gin from air to roll surface (convection zone 4)
I-J	radiation heat gain to the roll from hot strip (radiation zone 2)
J-A	heat gain due to conduction from strip to roller (conduction zone 1)

The analysis of cooling requires one to calculate the heat transfer equation from the roll. To cool the surface of the work rolls, water is supplied from nozzles, which are located at the exit and entry sides of the stands. Work rolls in finishing stands of the hot rolling mill are equipped with cooling nozzles both at the exit and entry sides of the stands. The work roll thermal model is capable to accommodate different cooling zones around the circumference of the work roll. Heating of the roll happens when it comes into contact with the strip or in the roll bite region J-A (Figure 3.3) and by radiation from strip to roll in region A-B and I-J. Following these regions, there is a zone of air cooling. After passing the air cooling region B-C, D-E, F-G, and H-I, the circumference of the roll is cooled by the water jet C-D, and G-H, respectively. Work-roll cooling takes place by convection due to air cooling (B-C, D-E, F-G, and H-I) and water cooling from the spray water (C-D, and G-H). Various arrangements of cooling can be followed depending on the water spray location and air cooling. Figure 3.3 shows the different divisions of the total roll circumference of 360 degrees along with typical cooling arrangements. Different heat transfer regimes along the surface of the roll have been introduced into the model by the incorporation of different values of heat transfer coefficient. All the calculation and theory is based on these zone divisions. Different boundary conditions and calculations are provided to each zone as consider as individual. Final analysis is done on the basis of these calculations. It was a coupled effect of all zonal behaviour and boundary conditions at the same time interval. The main assumptions for the model are:

- Heat conduction of roll and strip is considered only along the radial and axial direction of the work roll
- The work roll and strip are assumed to be of homogeneous material
- Small portion of the roll barrel length is only considered for these analysis due to symmetry of nature
- Maximum 5 revolution only considered and it assume that the thermal profile become converged

- Each zones calculation is done on the basis of maximum temperature and thermal load conditions.

3.1 Conduction and Radiation model

3.1.1 Analytical solution method

Conduction Model

The heat transfer from the work roll has been modelled using three dimensional axis symmetric transient conduction equations in cylindrical coordinates, where r is defined along the radial direction, z along axial direction and θ along angular direction. Using Eulerian description and assuming constant thermal properties, mathematical formulation governing the transient temperature field, $T(r, \theta, z)$ for a homogeneous and isotropic work roll is given by

$$k\left(\frac{\partial^2 T}{\partial r^2} + \frac{1}{r}\frac{\partial T}{\partial r} + \frac{1}{r^2}\frac{\partial^2 T}{\partial \theta^2} + \frac{\partial^2 T}{\partial z^2}\right) + \dot{q} = \rho c \frac{\partial T}{\partial t} \tag{3.1}$$

Here there is no internal heat generation $\dot{q}$ within the rolls during rolling. Therefore, $\dot{q} = 0$. Numerical solution of Equation 3.1 can be estimated by the finite element procedure that is applied on a slice of a unit circumferential depth. The temperature variation in circumferential direction of the work roll is ignored because work roll cycle time is much smaller than the response time of the rolling condition variations.

The temperature along the radius r and at the vertical distance z at time t is denoted by $T = T(r, z, t)$. We consider a radial and a vertical thermal process, rotationally symmetric around the z-axis. The interval along r is divided into a numerical mesh with the cell widths $\Delta r_i, i = 1, ..., N$. See Figure 3.4. The midpoint of cell i lies at $r = r_i$. The inner boundary lies at $r = r_-$, and the outer boundary lies at $r = r_+$. Note that r_- may be zero, i.e. at the z-axis. We have:

$$r_1 = r_- + \frac{\Delta r_1}{2} \; r_i = r_{i-1} + \frac{\Delta r_{i-1}}{2} + \frac{\Delta r_i}{2} \; i = 2, ..., N \tag{3.2}$$

The sum of the cell widths equals the total width of the annulus:

$$\sum_{i=1}^{N} \Delta r_i = r_+ - r_- \tag{3.3}$$

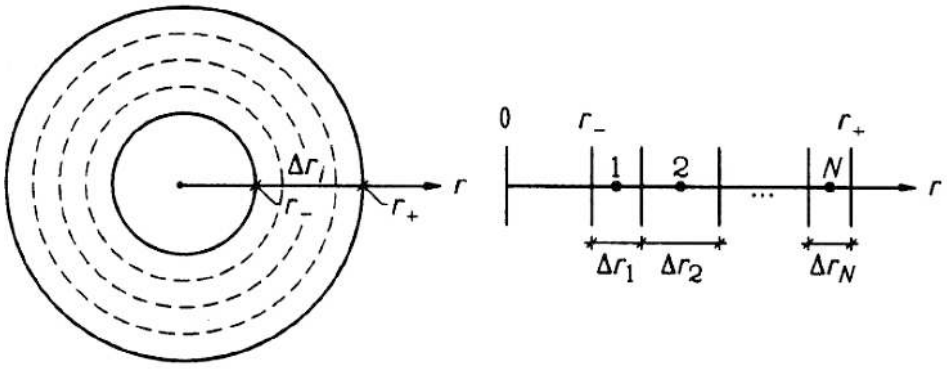

Figure 3.4: Mesh in the radial direction

In the z-direction, the cell widths are denoted by Δz_j. See Figure 3.5. The temperature at the midpoint of cell (i, j) at time step n is denoted $T_{i,j}$:

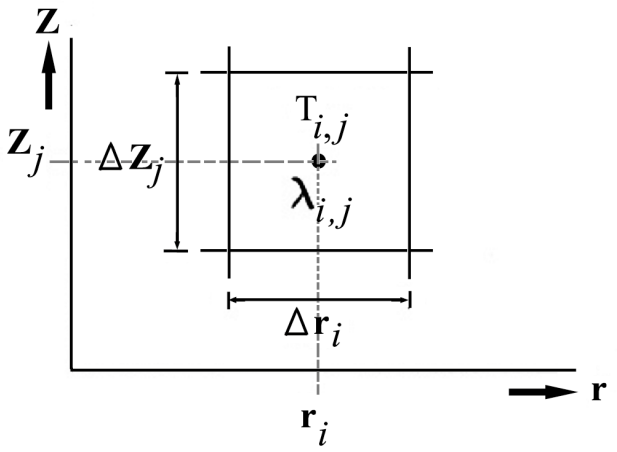

Figure 3.5: Mesh in cylindrical coordinates

$$T_{i,j} = T\left(r_i, z_j, n\Delta t\right) \tag{3.4}$$

The cell (i, j) is an annular ring of cylindrical shape:

$$cell(i,j) : r\_i - \Delta r_i/2 \leq r \leq r_i + \Delta r_i/2 \; z_i - \Delta z_i/2 \leq z \leq z_i + \Delta z_i/2 \tag{3.5}$$

The volume becomes:

$$\left[\pi\left(r_i + \Delta r_i/2\right)^2 - \pi\left(r_i - \Delta r_i/2\right)^2\right]\Delta z_j = 2\pi r_i \Delta r_i \Delta z_j \tag{3.6}$$

The conductance between cell $(i-1, j)$ and (i, j) is:

$$K_{i-0.5,j} = \frac{\Delta z_j}{\frac{1}{2\pi\lambda_{i-1,j}} ln\frac{r_{i-0.5}}{r_{i-1}} + \frac{1}{2\pi\lambda_{i,j}} ln\frac{r_i}{r_{i-0.5}} + \frac{R_{i-0.5,j}}{2\pi r_{i-0.5}}} \tag{3.7}$$

Here, the first of the three terms in the denominator is the thermal resistance (per unit height) of the annulus $r_{i-1} < r < r_{i-0.5}$. There may be an internal resistance $R_{i-0.5,j}$,(m^2K/W), at the interface between the cells.

The conductance in the z-direction is equal to the one-dimensional conductance multiplied by the area of the cell perpendicular to z, i.e. $2\pi r_i \Delta r_i$:

$$K_{i,j-0.5} = \frac{2\pi r_i \Delta r_i}{0.5\Delta z_{j-1}/\lambda_{i,j-1} + 0.5\Delta z_j/\lambda_{i,j} + R_{i,j-0.5}} (W/K) \tag{3.8}$$

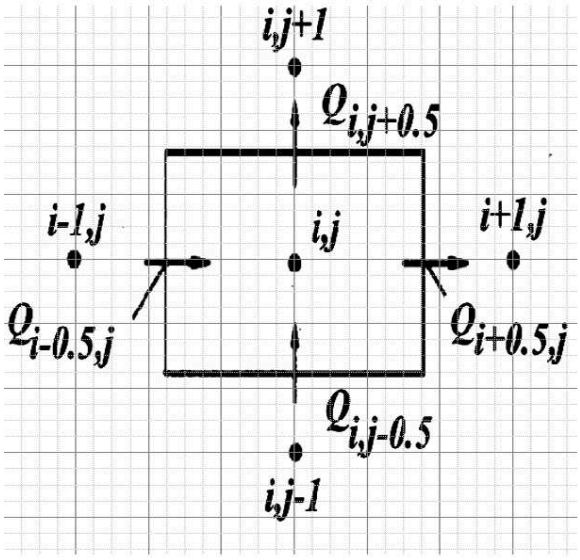

Figure 3.6: Definition of flows (W) to and from cell (i, j)

The heat flows, see Figure 3.6, are given by a conductance times the temperature difference. The flows become for all i and j:

$$\begin{aligned} Q_{i-0.5,j} &= K_{i-0.5,j}\left(T_{i-1,j} - T_{i,j}\right) \ all\ i\ and\ j \\ Q_{i,j-0.5} &= K_{i,j-0.5}\left(T_{i,j-1} - T_{i,j}\right) \ all\ i\ and\ j \end{aligned} \tag{3.9}$$

The heat balance equation becomes:

$$C_{i,j} 2\pi r_i \Delta r_i \Delta z_j \left(T_{i,j}^{new} - T_{i,j}\right) = \left[Q_{i-0.5,j} - Q_{i+0.5,j} + Q_{i,j-0.5} - Q_{i,j+0.5}\right] \Delta t \tag{3.10}$$

The criterion for numerical stability is:

$$\Delta t < \frac{C_{i,j} 2\pi r_i \Delta r_i \Delta z_j}{K_{i-0.5,j} + K_{i+0.5,j} + K_{i,j-0.5} + K_{i,j+0.5}} \ for\ all\ i\ and\ j \tag{3.11}$$

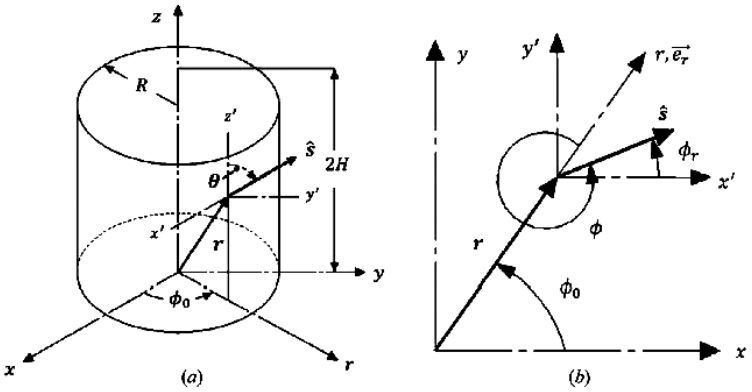

Figure 3.7: Schematics of the cylindrical system: (a) geometry and location of vectors with reference to Cartesian coordinate system; (b) definition of azimuthal angles.

Radiation Model

The time dependent governing equations of radiative heat transfer in cylindrical coordinates for a gray, absorbing-emitting and scattering medium is

$$\frac{1}{c}\frac{\partial I\left(r,\hat{s}\right)}{\partial t}+\frac{\partial I\left(r,\hat{s}\right)}{\partial s}=-\beta I\left(r,\hat{s}\right)+S\left(r,\hat{s}\right) \tag{3.12}$$

where $S\left(r,\hat{s}\right)$ is the source function and is

$$S\left(r,\hat{s}\right)=\sigma_a I_b\left(r,\hat{s}\right)+\frac{\sigma_s}{4\pi}\int_{4\pi} I\left(r,\hat{s}'\right)\phi\left(\hat{s}',\hat{s}\right)\mathrm{d}\Omega' \tag{3.13}$$

Eq. 3.12 is applied to the cylindrical enclosure shown in Figure 3.7. The vectors r and $\hat{s}$ are the position and unit direction vectors locating the radiative intensity, with direction cosines $\mu = sin\theta cos\phi$, $\eta = sin\theta sin\phi$ and $\xi = cos\theta$. The ERT for an axisymmetric cylindrical medium can be expressed as :

$$\frac{1}{c}\frac{\partial I}{\partial t}+\frac{\mu}{r}\frac{\partial}{\partial r}[rI]-\frac{1}{r}\frac{\partial}{\partial\phi}[\eta I]+\xi\frac{\partial I}{\partial z}=-\beta I+S \tag{3.14}$$

Using a control-volume approach, Eq. 3.14 is integrated over an arbitrary control volume, described by volume ΔV and solid angle $\Delta\Omega$. Following this integration, and application of Gausss theorem, Eq. 3.14 can be written, for a discrete direction m, as :

$$\begin{aligned}\frac{1}{c}\frac{\partial}{\partial t}\int_{\Delta\Omega^m}\int_{\Delta V}(I^m)\mathrm{d}V\mathrm{d}\Omega+\int_{\Delta\Omega^m}\int_{\Delta A}I^m(\hat{s}^m.\hat{n})\mathrm{d}A\mathrm{d}\Omega\\ =\int_{\Delta\Omega^m}\int_{\Delta V}\beta(-I^m+S^m)\mathrm{d}V\mathrm{d}\Omega\end{aligned} \tag{3.15}$$

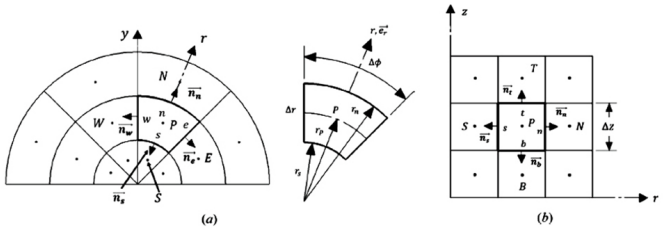

Figure 3.8: Schematics of a typical control-volume: (a) top view; (b) side view in rz plane

where $\hat{n}$ is the outward normal vector for a given surface. Using the important assumption that the intensity over a given control volume and solid angle remains constant, the integrals can be replaced by summations. Equation 3.15 can therefore be simplified, giving the following form:

$$\frac{1}{c}\frac{\partial I^m}{\partial t}\Delta V\Delta\Omega^m + \sum_{i=1}^{6} I_i^m \Delta A_i D_i^m = (-\beta I^m + \beta S^m)\Delta V\Delta\Omega^m \tag{3.16}$$

where the summation on the left-hand side is carried out over the six faces of the control volume. The typical control volume used for this analysis is shown in Figure 3.8. The discrete solid angle $\Delta\Omega^m$ is defined as

$$\Delta\Omega^m = \int_{\Delta\Omega^m} \mathrm{d}\Omega^m = \int_{\phi^{m-}}^{\phi^{m+}} \int_{\theta^{m-}}^{\theta^{m+}} sin\theta \mathrm{d}\theta\mathrm{d}\phi = (cos\theta^{m^-} - cos\theta^{m^+})(\phi^{m^+} - \phi^{m^-}) \tag{3.17}$$

where ϕ^{m^+}, ϕ^{m^-}, θ^{m^+} and θ^{m^-} are the azimuthal and polar angles defining the edges of the discrete solid angle, as shown in Figure 3.9. The source term is defined as :

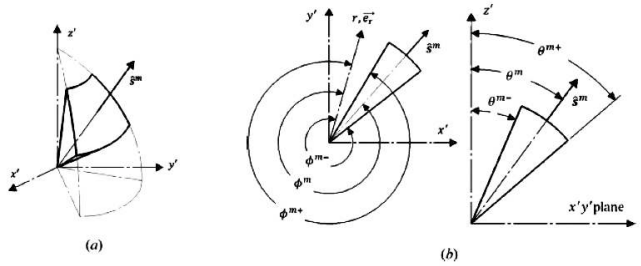

Figure 3.9: Schematics of the discrete solid angle: (a) location of 3-D solid angle; (b) definition of azimuthal and polar edge angles.

$$S^m = (1-\omega)I_b + \frac{\omega}{4\pi}\sum_{m'=1}^{M} \bar{\Phi}^{m'm} I^{m'} \Delta\Omega^{m'} \quad m = 1, 2.....M \tag{3.18}$$

where $\bar{\Phi}^{m'm}$ is the average scattering phase function from direction m' to direction m. The directional weight at control-volume face i in direction m, represented by the symbol D_i^m in Eq 3.16, can be calculated for each face using the following integral expansion:

$$D_i^m = \int_{\phi^{m^-}}^{\phi^{m^+}} \int_{\theta^{m^-}}^{\theta^{m^+}} (\hat{s}^m.\hat{n}_i) sin\theta \mathrm{d}\theta \mathrm{d}\phi \tag{3.19}$$

As an example, for the "north" face in the control volume shown in Figure 3.8 ($i = n$), the normal vector is $\hat{n}_n = \overrightarrow{e_r}$, and thus the dot product $\hat{s}^m.\hat{n}_n = sin\theta cos\phi$. Thus, the north directional weight is

$$D_n^m = (sin\phi^{m^+} - sin\phi^{m^-}) * [\frac{1}{2}(\theta^{m^+} - \theta^{m^-}) - \frac{1}{4}(sin2\theta^{m^+} - sin2\theta^{m^-})] \tag{3.20}$$

Calculations for all six faces are presented in detail by Kim

A special consideration is needed when describing the scattering phase function for this method. In order to satisfy all moment constraints, the discrete solid angles must be subdivided into smaller subangles. The average scattering phase function from a solid angle $\Delta\Omega^{m'}$ into a second solid angle $\Delta\Omega^m$ can be accurately calculated as

$$\bar{\Phi}^{m'm} = \frac{1}{\Delta\Omega^{m'}\Delta\Omega^m} \sum_{m_d=1}^{M_d} \sum_{m'_d=1}^{M'_d} \Phi^{m'_d m_d} \Delta\Omega^{m'_d} \Delta\Omega^{m_d} \tag{3.21}$$

where M_d and M'_d are the number of subdivisions in each discrete solid angle.

Similarly to the DOM, once the intensity field is found by solution of the governing equation, the total radiant heat fluxes at the radial side wall and axial end wall can be calculated using:

$$\begin{aligned} Q_r &= \sum_{m=1}^{M} I^m D_n^m \\ Q_z &= \sum_{m=1}^{M} I^m D_t^m \end{aligned} \tag{3.22}$$

Again, these summations are calculated over all directions m, accounting for both incoming and outgoing fluxes.

To obtain the discretized equation for the FVM, Eq 3.14 is expanded over the control volume in Figure 3.8. Analyzing the summations over the faces $i = n, s, e, w, t, b$ shown in Figure 3.8, the discretized form of Eq 3.14 becomes:

$$\frac{I_p^m - I_p^{m0}}{c\Delta t}\Delta V \Delta\Omega^m + \sum_{i=n,s,e,w,t,b} I_i^m \Delta A_i \Delta D_i^m = -\beta I_p^m \Delta V \Delta\Omega^m + \beta S_p^m \Delta V \Delta\Omega^m \tag{3.23}$$

where the partial derivative in time has been evaluated using a forward-differencing technique with I_p^{m0} as the nodal intensity from the previous time step, the subscript P represents the control-volume center, ΔA_i and ΔV are the facial area and control-volume, respectively.

Equation 3.23 is more readily solved if it is written in terms of neighbouring nodal intensities $i = N, S, E, W, T, B$ instead of facial intensities $i = n, s, e, w, t, b$. As outlined by Modest, there are many schemes that can be used to transform this equation into the desired form. In this treatment, the simple step scheme was used (as in the DOM, for consistency). This scheme will ensure positive intensities. The following replacements are made for this scheme in Eq 3.23:

$$I_i^m D_i^m = I_P^m max(D_i^m, 0) - I_I^m max(D_i^m, 0) \tag{3.24}$$

The faces $I = e, w$ get a special treatment. In the step scheme, the west facial intensity is a known quantity. This is due to the sweeping scheme, where the west face on the current control volume is equal to the east face on the previous control volume. The east facial intensity is unknown, and is approximated in the step scheme as the intensity at the center of the current control volume. Using these approximations, Eq 3.23 can be rewritten in the desired form

$$\alpha_P^m I_P^m = \sum_{I=N,S,T,B} \alpha_I^m I_I^m - \Delta A_W D_W^m I_P^{m-1} + \beta S_P^m \Delta V \Delta\Omega^m + \frac{\Delta V \Delta\Omega^m}{c\Delta t} I_P^{m0} \tag{3.25}$$

where the superscript $m-1$ designates that the nodal intensity be taken from

the previous control volume in the

$$\alpha_P^m = \frac{\Delta V \Delta \Omega^m}{c\Delta t} + \sum_{i=n,s,t,b} max(\Delta A_i D_i^m, 0) + \beta \Delta V \Delta \Omega^m + \Delta A_e D_e^m$$

$$\alpha_I^m = max(-\Delta A_i D_i^m, 0)$$

$$S_P^m = (1-\omega) I_b + \frac{\omega}{4\pi} \sum_{m'=1}^{M} \bar{\Phi}^{m'm} I_P^{m'0} \Delta \Omega^{m'} \tag{3.26}$$

The above equations, along with the necessary boundary and initial conditions, provide the framework for the solution of the ERT with the FVM.

As previously mentioned, for an axisymmetric geometry, the intensities are invariant with the spatial azimuthal angle ϕ_0. Thus, by fixing a value of ϕ_0, the intensities corresponding to the vector $\hat{s}$ can be obtained by simply solving the discretized equations at different values of ϕ_r. However, as discovered by Chui and Raithby, this method introduces a lack of conservation and unphysical directional coupling. To avoid this, they introduced a simple mapping solution. Instead of fixing ϕ_0, the value of ϕ_r for all intensity vectors was set to zero. The directional intensities were then calculated by solving the discretized equations at various values of ϕ_0.

The cylindrical geometry was divided into $(N_r \times N_z)$ equally spaced control volumes. The total solid angle of 4π was divided into $(N_\phi \times N_\theta)$ equally spaced directions, with $\Delta\theta = \pi/N_\theta$ and $\Delta\phi = \pi/N_\phi$. The intensities for all points were solved by sweeping in the θ and ϕ directions. There are four possible sweep directions, corresponding to the values of the directional weights in the radial and axial directions. For example, if D_n^m and D_t^m are both positive, the solution procedure will sweep from the radial centerline out to the radial side wall, and from the bottom end wall to the top end wall $(r = 0 \rightarrow R, z = 0 \rightarrow 2H)$. Finally, the intensity distribution in the medium is symmetric about the axis $y = 0$. This means that only the control volumes where $y \geq 0$ need be solved.

3.1.2 Simulation and analysis solver preference

For the symmetry of geometrical shape of the work roll and to save the calculation time, only a portion of work roll is simulated in this model. The simulation

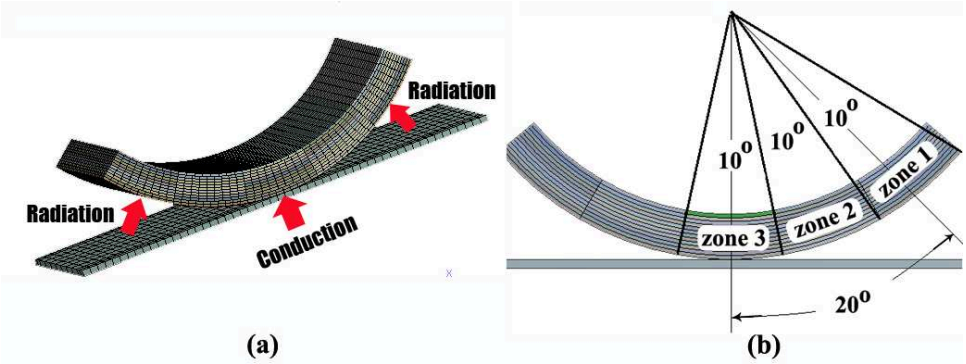

Figure 3.10: [a] schematic representation of heat flow by radiation and conduction. [b] Schematic representation of different zones of conduction and radiation

is carried out for both steady state and transient conditions with a time period of one second. Literatures cite that the temperature effect and heat flow variations is significant only within the nearest layer of roll surface. Therefore, instead of a complete cylindrical work roll, a portion of hollow cylinder with the same diameter and a thickness of 100mm are considered for this simulation as shown in Figure 3.10. The diameter of the roll is 800mm and the thickness of the hot metal slab is 12mm. Variation of mechanical quantities such as stress, strain etc.., and thermal expansion of strip and heat generated due to the plastic deformation of the strip material is not considered during simulations.

Boundary Conditions

- From the metal strip, a constant heat flux of 106 W/m^2 with a temperature of 1150^0C is generated.
- Ambient Temperature $\Rightarrow 27^0C$.
- Emissivity of roller $\Rightarrow$ 0.89.

The main objective here is to find out temperature and heat flow variation is angular and radial direction of the work roll surface by the effect of conduction and radiation heat transfer. Thus the angular nodal distribution of thermal profiles can be generated so as to use in the next phase analysis. ANSYS 13-Workbench Transient Thermal and Steady State Thermal module is used for this analysis. Here the solver is mechanical APDL.

3.2 Convection model

3.2.1 Analytical solution method

The governing one dimensional equations for heat transfer in cylindrical coordinates is

$$\frac{1}{r}\frac{\partial}{\partial r}\left(kr\frac{\partial T}{\partial r}\right)+g=\rho c\frac{\partial T}{\partial r} \tag{3.27}$$

where k represents the thermal conductivity, g the rate of heat generation per unit volume, ρ the density, and c the specific heat capacity. The heat generated term, g, was incorporated to give completeness to the model for cooling steel rods. The justification for assuming one dimensional heat conduction from the roller lies in the fact that circumferential and axial variation of convective heat transfer from the roll surface is insignificant.

$$\begin{aligned} -k\frac{\partial T}{\partial r} &= h\left(T-T_{\alpha}\right) r=R, t>0 \\ \frac{\partial T}{\partial r} &= 0 \; r=0, t>0 \\ T &= T_i \; 0\leq r\leq R, t=0 \end{aligned} \tag{3.28}$$

where R is the radius of the rod and h is the heat transfer coefficient, representing the net effect of convection and radiation heat losses. For the solution of the Equation 3.27, the finite element method was chosen, as stability in the transient analysis can be achieved using fewer nodes as compared to, for example, the explicit finite difference scheme. This also implies that the computational time required in the finite element scheme is lower. Equation 3.27 can be recast to yield the following weighted integral form :

$$\int_0^1\int_0^{\frac{\pi}{8}}\int_{ra}^{rb}\omega\left[-\frac{1}{r}\frac{\partial}{\partial r}\left(kr\frac{\partial T}{\partial r}\right)+\rho c\frac{\partial T}{\partial t}-g\right]r\mathrm{d}r\mathrm{d}\theta\mathrm{d}z=0 \tag{3.29}$$

where ω is the weight function and ra and rb are the coordinates of atypical element. Equation 3.29 can be rewritten as:

$$\frac{\pi}{8}\int_{ra}^{rb}\omega\left[-\frac{1}{r}\frac{\partial}{\partial r}\left(kr\frac{\partial T}{\partial r}\right)+\rho c\frac{\partial T}{\partial t}-g\right]r\mathrm{d}r=0 \tag{3.30}$$

The weak form of Equation 3.30 where differentiation is shared equally between ω and T is:

$$0 = \int_{ra}^{rb} \left(kr \frac{\partial T}{\partial r} \frac{\partial \omega}{\partial r} + \omega \rho c r \frac{\partial T}{\partial t} - \omega g r \right) \mathrm{d}r - \omega(rb) Q_B - \omega(ra) Q_A \tag{3.31}$$

where

$$\begin{aligned} Q_B &= \frac{\pi}{8} \left(kr \frac{\partial T}{\partial r} \right)_{rb} \\ Q_A &= -\frac{\pi}{8} \left(kr \frac{\partial T}{\partial r} \right)_{ra} \end{aligned} \tag{3.32}$$

The primary variable T in Equation 3.31 is approximated by the following polynomial of order n

$$T \approx \sum_{j=1}^{n} u_j(t) \psi_j(r) \tag{3.33}$$

where u_j is the value of the primary variable at the j^{th} node and ψ_j is the value of the interpolation function at this node. The interpolation functions are of the Lagrange type and also serve as the weight functions for the development of the required number of equations. The i^{th} equation, for which $\omega = \psi_i$, can be stated as :

$$0 = \int_{ra}^{rb} \left(kr \sum_{j=1}^{n} u_j \frac{\mathrm{d}\psi_j}{\mathrm{d}r} \frac{\mathrm{d}\psi_i}{\mathrm{d}r} + \psi_i \rho c r \sum_{j=1}^{n} \psi_j \frac{\mathrm{d}u_j}{\mathrm{d}t} - \psi_i g r \right) \mathrm{d}r - Q_i \tag{3.34}$$

Since $\sum_{j=1}^{n} \psi_i(r_j) Q_j = Q_i$, Equation 3.34 can be recast as :

$$0 = \sum_{j=1}^{n} u_j \int_{ra}^{rb} kr \frac{\mathrm{d}\psi_j}{\mathrm{d}r} \frac{\mathrm{d}\psi_i}{\mathrm{d}r} \mathrm{d}r + \sum_{j=1}^{n} \frac{\mathrm{d}u_j}{\mathrm{d}t} \int_{ra}^{rb} \rho c r \psi_i \psi_j \mathrm{d}r - \left[\int_{ra}^{rb} \psi_i g r \mathrm{d}r + Q_i \right] \tag{3.35}$$

or

$$0 = \sum_{j=1}^{n} K_{ij} u_j + \sum_{j=1}^{n} M_{ij} \frac{\mathrm{d}u_j}{\mathrm{d}t} - F_i \tag{3.36}$$

where

$$K_{ij} = \int_{ra}^{rb} kr \frac{\mathrm{d}\psi_j}{\mathrm{d}r} \frac{\mathrm{d}\psi_i}{\mathrm{d}r} \mathrm{d}r \, M_{ij} = \int_{ra}^{rb} \rho c r \psi_i \psi_j \mathrm{d}r \, F_i = \int_{ra}^{rb} \psi_i g r \mathrm{d}r + Q_i$$

In matrix form, the element equation can be stated as:

$$\lfloor K^e \rfloor \{u^e\} + \lfloor M^e \rfloor \{\dot{u}^e\} \tag{3.37}$$

where $\dot{u}$ represents the time derivative of u, the primary variable, and e is the element under consideration. For the approximation of the time derivative, the alpha family of time approximation was invoked. In this, the weighted average of the time derivative of the variable at two successive time instants is approximated by a linear interpolation of the values of the variable at two instants.

$$(1-\alpha)\{\dot{u}\}_s + \alpha\{\dot{u}\}_{s+1} = \frac{u_{s+1}-u_s}{\Delta t_{s+1}} \; 0 \leq \alpha \leq 1 \tag{3.38}$$

Equation 3.38 can be stated for two successive time instants s and $s+1$ as:

$$[M]_s\{\dot{u}\}_s + [K]_s\{u\}_s = F_s \tag{3.39}$$

$$[M]_{s+1}\{\dot{u}\}_{s+1} + [K]_{s+1}\{u\}_{s+1} = F_{s+1} \tag{3.40}$$

Utilizing Equation 3.38, Equation 3.39 and Equation 3.40 and the fact that $[M]_s = [M]_{s+1} = [M]$, $\{\dot{u}\}$ can be eliminated from Equation 3.37 to yield the following equation :

$$\Delta t_{s+1}\alpha\left[\{F\}_{s+1} - [K]_{s+1}\{u\}_{s+1}\right] + \Delta t_{s+1}(1-\alpha)\left[F_s - [K]_s\{u\}_s\right] = [M](\{u\}_{s+1} - \{u\}_s) \tag{3.41}$$

From Equation 3.41 it is evident that from a knowledge of the value of the primary variable at a time instant s, the value at the succeeding time instant $s+1$ can be easily evaluated. The element equations were assembled using the concept of balance of heat flux at the connecting nodes and the single-valued nature of the primary variable. The evaluation of the coefficient matrices required the use of a numerical integration technique. The Gauss-Legendre quadrature was used for that purpose, as it involves fewer quadrature points than other quadrature rules. The solution of equations was done using Gauss-elimination technique.

3.2.2 Simulation and analysis solver preference

The main objective of this phase is to find out the convective heat transfer coefficient and temperature variation of the roll surface and fluid interface. A thin layer of cylindrical surface with same roll diameter is considered for this analysis

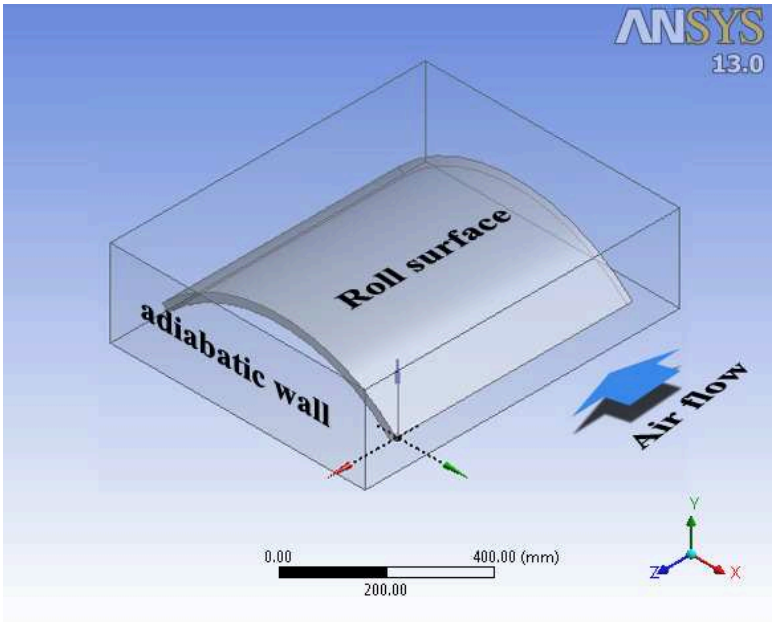

Figure 3.11: The computational and physical domain and boundary conditions of convective air cooling

as shown in Figure 3.11. The solution domain is filled with air. All the computational fluid dynamics (CFD) criteria are incorporated into this phase. The flow of air is assumed to be steady, incompressible and three dimensional. The fluid domain is considered as air and it is moving with a velocity equivalent to the linear velocity of roller as per the industrial specification while the roller part is kept as stationary with a heat emitting surface. This model is solved using CFD software (ICEM mesher and CFX solver) which are combined with continuity and momentum equation to simulate turbulence flow and thermal fields.

Boundary Conditions

- The bottom wall of solid domain is considered to be the heat source and top surface of the wall is heat sink.
- It is assumed that, heat is generated from the heat source at a uniform rate and can be represented by a constant heat flux.
- The four side faces of the solid domain are kept as adiabatic.
- A constant velocity of air flow is given through one face wall of fluid domain as inlet and opposite face wall is considered as opening with a relative pres-

sure of zero Pascal and remaining walls of fluid domain are kept as stationary no slip wall

3.3 Combined Heating model (radiation, conduction and convection)

3.3.1 Analytical solution method

The heat transfer in the cylinder is assumed to be two dimensional. The temperature is denoted as $T(\rho, \varphi)$. The physical parameters of the problem are summarized in Figure 3.12. According to the physical conditions described previously, the governing equations can be written as :

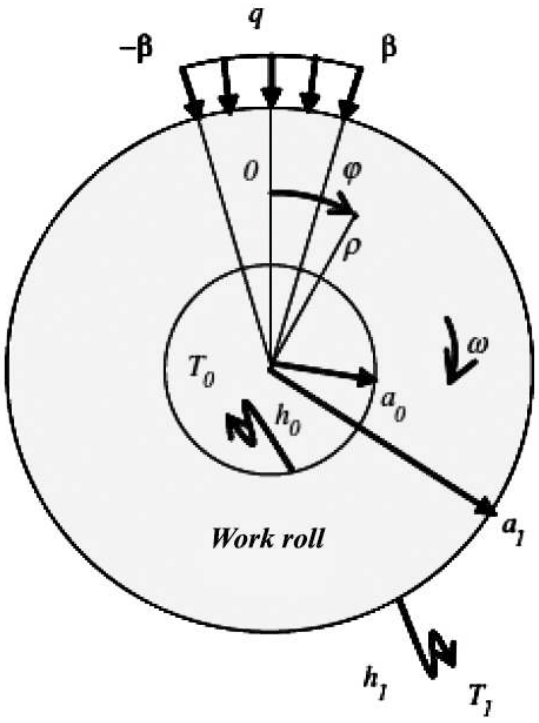

Figure 3.12: Simplified scheme of the roller (physical parameters)

$$\frac{\partial^2 T}{\partial \rho^2} + \frac{1}{\rho}\frac{\partial T}{\partial \rho} + \frac{1}{\rho^2}\frac{\partial^2 T}{\partial \varphi^2} - \frac{\omega}{\alpha}\frac{\partial T}{\partial \varphi} = 0 \tag{3.42}$$

The last term of the left-hand side of Equation 3.42 represents the relative motion of the cylinder with respect to the heat source q. It is the convection term whose importance depends on the values of the angular velocity ω and the thermal

diffusivity α. The boundary conditions with respect to the radial direction ρ are given by:

$$\lambda\frac{\partial T}{\partial \rho} = q(\rho = a_1, -\beta \leq \varphi\beta)$$

$$\lambda\frac{\partial T}{\partial \rho} = -h_1(T(\rho,\varphi) - T_1)(\rho = a_1, -\pi \leq \varphi \leq -\beta \; and \; \beta \leq \varphi\pi) \tag{3.43}$$

$$\lambda\frac{\partial T}{\partial \rho} = h_0(T(\rho,\varphi) - T_0)(\rho = a_0, -\pi \leq \varphi \leq \pi) \tag{3.44}$$

The first and the second parts of Equation 3.43 are the heat flux entering through the rollerworkpiece contact area ($-\beta \leq \varphi \leq \beta$) and the external convection cooling ($-\pi \leq \varphi \leq -\beta \; and \; \beta \leq \varphi\pi$), respectively. The heat convection coefficient is h_1 and the ambient temperature T^1. For the internal face, cooling is homogeneous on the entire surface. The heat convection coefficient and the ambient temperature in this part are, respectively, denoted by h_0 and T_0. The heat transfer is periodic along the angular direction. The periodicity conditions can be written as

$$T(\rho, -\pi) = T(\rho, \pi) \tag{3.45}$$

$$\frac{\partial T(\rho, -\pi)}{\partial \varphi} = \frac{\partial T(\rho, \pi)}{\partial \varphi} \tag{3.46}$$

3.3.2 Simulation and analysis solver preference

In this model conduction, radiation and convection phases of the previous model are combined to find out the total heat transfer effect and temperature profile by heating. It is a complete heating model. Extensive simulations were carried out by varying physical and dynamic parameters of the work roll. The simulation is carried out with both steady state and transient conditions. Two approaches are used for solving this definite model.

- Approach 1 : The heat flow from the strip is considered as a moving heat source along the circumferential directions of the roller. For simplicity the roller is considered as a different angular sector as shown in Figure 3.13. The angular direction of the moving heat source is opposite to the angular rotation of the roller. The angular displacement of the moving heat source

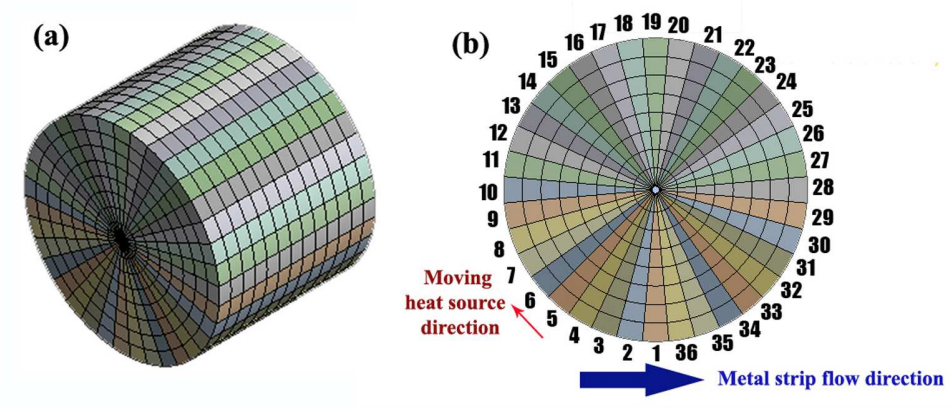

Figure 3.13: [a]meshed form of work roll with 36 angular division in approach 1 [b] Boundary conditions and description of heat moving source

is depending on the angular velocity of the roller. The time interval for each heat source angular displacement is always equal to the ratio of total time taken for one revolution and total number of angular sectors.

$$\Delta t = \frac{Totaltime}{Numberofangularsectors} \tag{3.47}$$

- Approach 2 : The virtual representation and simulation of the hot rolling process is carried out in this approach. Here, the physical visualization of this virtual plate and the roller is as shown in Figure 3.14. Here, the roll part of the body is kept stationary and the strip is moving across the boundary of the roller considering it as a virtual plate. The real physics of this simulation is to approximate practical scenario. Even though the reverse process of the exact hot rolling process is performed here, but the net effect is the same because the thermal expansion, thermal variation and the mechanical profile of the strip is not considered in this simulations. Different virtual plates are provided here with respect to the predicted rotation speed of the roller. At a time, only one plate is activated. The activation time duration is calculated by the equation

$$ActivationTime/Timeinterval = \frac{Totaltimetakenforonerevolution}{Totalnumberofvirtualplates} \tag{3.48}$$

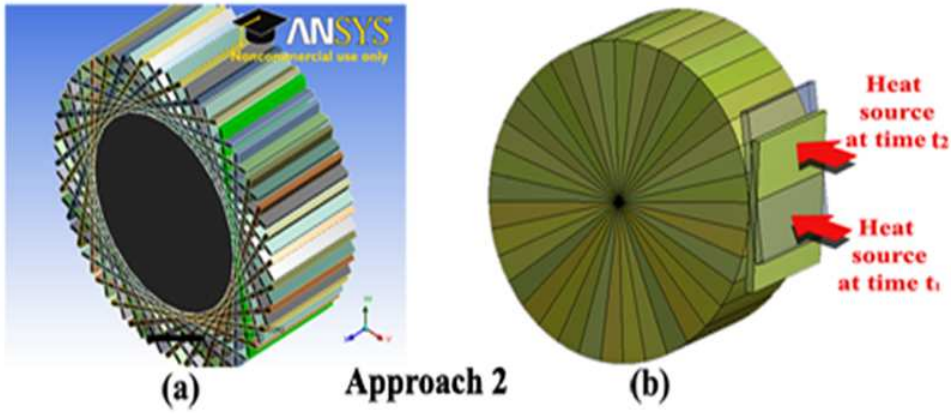

Figure 3.14: [a] physical description of virtual moving plate. [b] Boundary conditions and description of heat moving source (hot virtual plate motion) with respect to time

The boundary condition specified for a particular plate at a particular time interval is shifted to adjacent plate in the next time interval. This model is simulated by mechanical ADPL solver in ANSYS 13 workbench.

3.4 Forced Cooling Model

3.4.1 Analytical solution method of Jet Impingement heat transfer on a cylindrical surface

Having assessed data from several sources, the following correlation for a single round nozzle ($A_r = D^2/4r^2$) is recommended :

$$\frac{\bar{Nu}}{Pr^{0.42}} = G\left(A_r, \frac{H}{D}\right)\left[2Re^{1/2}\left(1 + 0.005Re^{0.55}\right)^{1/2}\right] \tag{3.49}$$

where

$$G = 2A_r^{1/2}\frac{1 - 2.2A_r^{1/2}}{1 + 0.2\left(H/D - 6\right)A_r^{1/2}} \tag{3.50}$$

The ranges of validity are

$$\begin{bmatrix} 2000 \lesssim R_e \lesssim 400000 \\ 2 \lesssim H/D \lesssim 12 \\ 0.004 \lesssim A_r \lesssim 0.004 \end{bmatrix} \tag{3.51}$$

For $A_r \gtrsim 0.004$ results for $\bar{Nu}$ are available in graphical form.

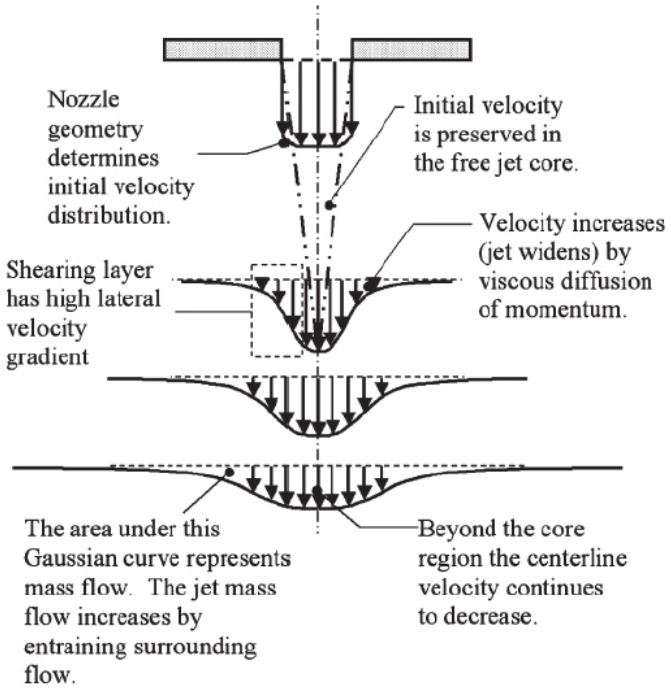

Figure 3.15: The flow field of a free submerged jet [42]

For an array of round nozzles ($A_r = \pi D^2/4S^2$ or $\pi D^2/2\sqrt{3}S^2$ for inline and staggered arrays, respectively),

$$\frac{\bar{Nu}}{Pr^{0.42}} = 0.5K\left(A_r, \frac{H}{D}\right) G\left(A_r, \frac{H}{D}\right) Re^{2/3} \tag{3.52}$$

where

$$K = \left[1 + \left(\frac{H/D}{0.6/A_r^{1/2}}\right)^6\right]^{-0.05} \tag{3.53}$$

and G is the single nozzle function given by Equation 3.50. The function K accounts for the fact that, for $H/D \gtrsim 0.6/A_r^{1/2}$, the average Nusselt number for the array decays more rapidly with increasing H/D than for a single nozzle. The correlation is valid over the ranges

$$\begin{bmatrix} 2000 \lesssim R_e \lesssim 100000 \\ 2 \lesssim H/D \lesssim 12 \\ 0.004 \lesssim A_r \lesssim 0.004 \end{bmatrix} \tag{3.54}$$

The flow of a submerged impinging jet passes through several distinct regions. The jet emerges from a nozzle or opening with a velocity and temperature profile

and turbulence characteristics dependent upon the upstream flow. After it exits the nozzle, the emerging jet may pass through a region where it is sufficiently far from the impingement surface to behave as a free submerged jet. Here, the velocity gradients in the jet create a shearing at the edges of the jet which transfers momentum laterally outward, pulling additional fluid along with the jet and raising the jet mass flow, as shown in Figure 3.15. If the shearing layer expands inward to the center of the jet prior to reaching the target, a region of core decay forms. For purposes of distinct identification, the end of the core region may be defined as the axial position where the centerline flow dynamic pressure (proportional to speed squared) reaches 95 percent of its original value. This decaying jet begins four to eight nozzle diameters or slot-widths downstream of the nozzle exit. In the decaying jet, the axial velocity component in the central part decreases, with the radial velocity profile resembling a Gaussian curve that becomes wider and shorter with distance from the nozzle outlet. In this region, the axial velocity and jet width vary linearly with axial position. Martin [41] provided a collection of equations for predicting the velocity in the free jet and decaying jet regions based on low Reynolds number flow. Viskanta [43] further subdivided this region into two zones, the initial developing zone, and the fully developed zone in which the decaying free jet reaches a Gaussian velocity profile.

3.4.2 Simulation and analysis solver preference

The solution domain is filled with ambient air. The three dimensional Navier Stokes and energy equations with the standard turbulence model are solved using CFD software (CFD mesher and CFX solver) which are coupled with continuity and momentum equations to simulate turbulence flow and thermal fields. The turbulence model used is shear stress transport (SST) k-w model which is found to work the most excellent among the available turbulence models for this flow configuration and is also chosen due to its simplicity, computational economy and wide acceptability. The flow is assumed to be three dimensional, steady and incompressible. The radiation heat transfer effects and buoyancy are neglected and thermo physical properties of the fluid such as specific heat, thermal conductivity

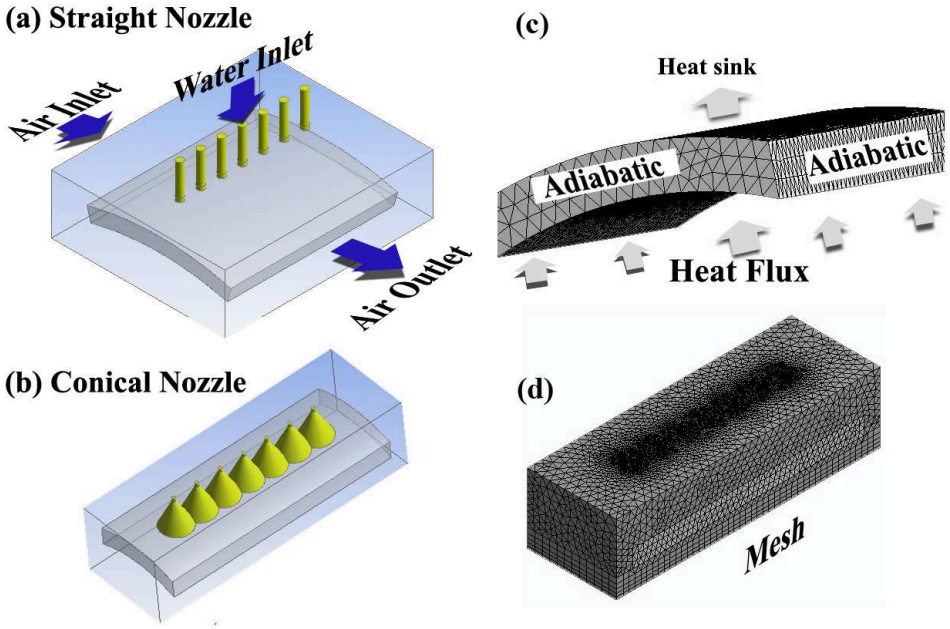

Figure 3.16: The computational, physical domain and boundary conditions of forced convective water jet cooling [a] straight nozzle arrangement [b] conical nozzle arrangement [c] work roll boundary conditions [d] mesh domain of multi jet impingement

and density are assumed to be constant. A thin layer of cylindrical solid with same roll diameter is considered for this analysis. The schematic diagram of the physical geometry and the computational domain is shown in the Figure 3.16(a) and Figure 3.16(b). The bottom wall of the solid domain is considered to be bottom surface of heat sink base. It is assumed that heat is generated inside heat sink base at constant rate and can be represented by a constant heat flux from the bottom surface of the heat sink. Water flow at high velocity passes through a round array jets with length l=25mm and diameter d=10mm, vertically impinging on the target surface. The jet after impingement will exit from opening. The bottom surface of roller part was kept at constant temperature of 900oc and except top surface all other walls are adiabatic. The details of plate geometry are shown in Figure 3.16(c). As geometry is small enough and we have sufficient computational power so here consider complete geometry for the CFD analyses and created in ANSYS CFX 13. The opening boundary is sufficiently away from the actual physics so that flow becomes stable and actual flow phenomenon at impinging surface is captured. The structural mesh was created within this domain

by using ANSYS CFD with the option of blocking. As structured mesh used the orthogonality is maintained, hence accurate prediction of heat transfer characteristics is possible. Hexa mesh is used over the entire computational domain and to predict the near wall flow phenomenon the dense hexa mesh is used as shown in Figure 3.16(d). This will not only capture the near wall flow phenomenon but also increase the smoothness of the mesh. Dense mesh also helps to control the y+. Grid independency on heat transfer characteristics is checked by changing the element size from 0.15 million to 1.1 million which follows that about 0.72 million was good enough for present analysis from view point of accuracy and computational time. The numerical simulations are carried out using the commercial CFD solver ANSYS CFX version 13. The flow and turbulence fields have to be accurately solved to obtain reasonable heat transfer predictions. Higher resolution scheme is used for all terms that affect heat transfer. Higher order discretization scheme is used for the pressure, momentum, turbulence kinetic energy, specific dissipation rate, and the energy. Flow, turbulence, and energy equations have been solved. In the fluid domain the inlet boundary condition is specified the measured velocity and static temperature (300K) of the flow were specified at the inlet of the nozzle. No-slip condition was applied to the wall surface. In fluid domain there is also opening boundary condition in which flow regime is subsonic, relative pressure is 0 Pa with the details of operating temperature (300K) and the turbulence intensity of 5 percent. In solid domain the constant heat flux was given with the initial temperature condition automatic with the base of heat sink and the sides of heat sink base plat are adiabatic. To simplify the solution, the variation of thermal and physical properties of water and air with temperature is neglected. The flow field was numerically examined by use of CFX (ANSYS), assuming the steady-state flow condition. A geometry and mesh object is imported into CFX CFD software environment for solving governing equations. The flow and turbulence fields have to be accurately solved to obtain reasonable heat transfer predictions. Second order scheme is used for all terms that affect heat transfer. Second order discretization scheme is used for the pressure, second order

upwind discretization scheme is used for momentum, turbulence kinetic energy, specific dissipation rate, and the energy. Flow, turbulence, and energy equations have been solved. To simplify the solution, the variation of thermal and physical properties of air with temperature is neglected. The standard SIMPLE algorithm is adopted for the pressure velocity coupling. The simulation type is steady state condition, convergence criteria are specified as 10E-05 residuals and convergence control is set at maximum 1000 iterations which can be changed if convergence is not achieved. Extensive simulations are carried out by varying nozzle parameters such as nozzle to target distance, velocity, working pressure and type of nozzles (straight and conical).

4 Results and Discussion

4.1 Conduction and Radiation Model

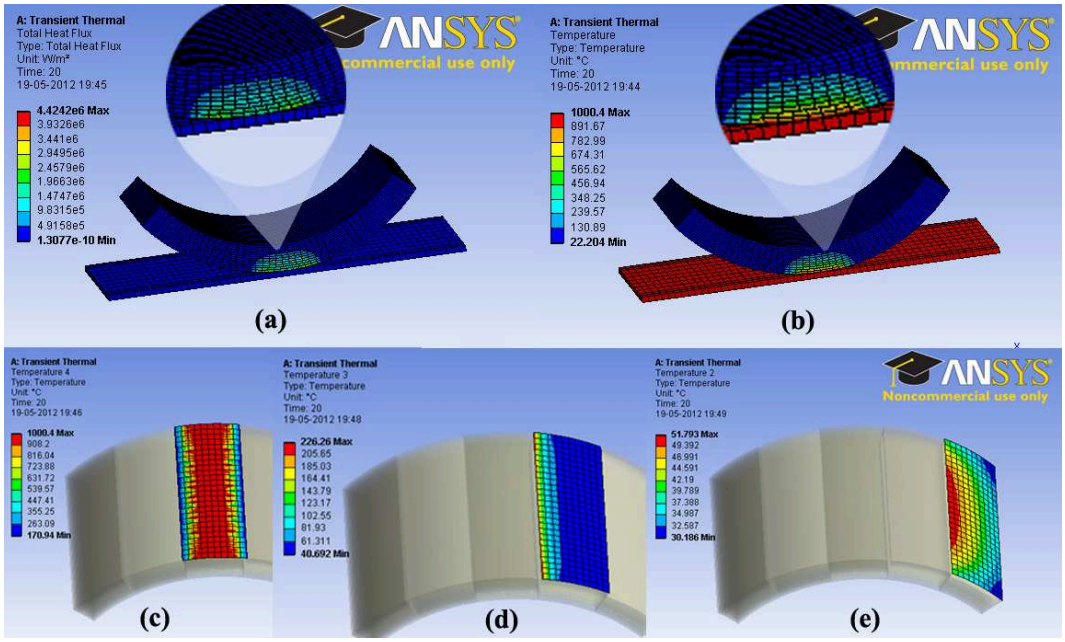

Figure 4.1: [a] Heat flux contour of conduction Radiation model [b] temperature contour of conduction Radiation model [c], [d] and [e] temperature contour of zone 3, zone 2 and zone 1 respectively

Conduction and radiation simulation has been carried out to obtain the temperature profile and the heat distribution of the roll. The description and various depending parameters are discussed in Section 3.1. The total temperature distribution and heat flux variation on the surface of roller is shown in Figure 4.1. From the figure the maximum heat transfer is occurring in the roll bite region of work roll. This model is divided into 3 zones. Each zone is created on the basis of 100 angular revolution of the surface body such as zone 1 zone 2 and zone 3.

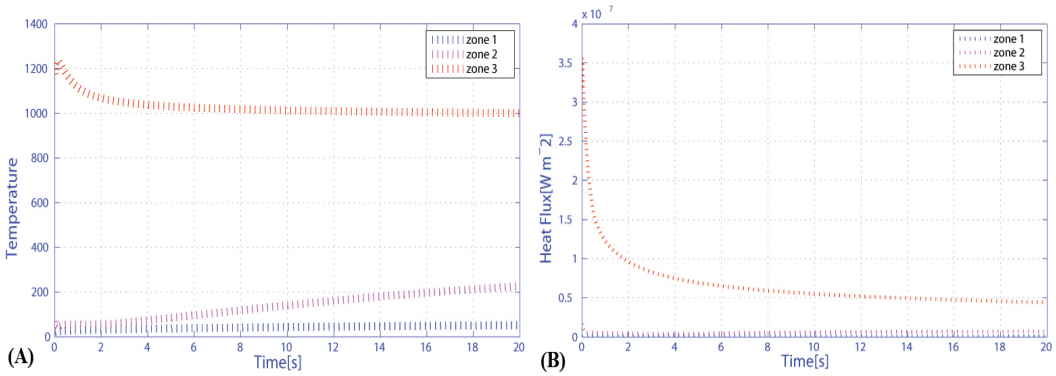

Figure 4.2: [a] temperature distribution of different zones with respect to time [b] Heat flux distribution of different zones with respect to time

The distribution of temperature at different zones is shown in Figure 4.2. With the influence of shape factor radiation rate will be varying with zone 3 to zone 1. The roll bite region is the only contact area in between roll and metal strip and hence heat transfer through conduction happens in this region only. During the initial stages of simulation the temperature difference between work roll and metal strip is very high near to 1120^0C. Therefore high amount of heat transfer will occur. At this stage the temperature of the roll surface in the roll bite region is increased to 927^0C rapidly. After one or two revolutions, the temperature of the roller is gradually increased then than initial temperature by the effect of thermal accumulation. Therefore the heat transfer rate is decreased which is shown in Figure 4.2(b).

Zonal wise temperature variation is plotted in Figure 4.2(a). From the result it is clear that the temperature variation in zone 1 is negligible. So it is clear that the heat transfer variation by conduction and radiation is affected only up to an angle of 20^0C circumferentially from the line of contact as shown in Figure 3.10(b).

The temperature distribution in the radial direction with varying depth from surface of the roller is plotted in Figure 4.3, where x1, x2, x3, x4, x5, x6, x7, x8, x9 and x10 be different points from the surface in radial direction with 5mm, 10mm, 15mm, 20mm, 25mm, 30mm, 35mm, 40mm, 45mm and 50mm respectively. This analysis is done with time duration of 20 seconds. From the result the temperature

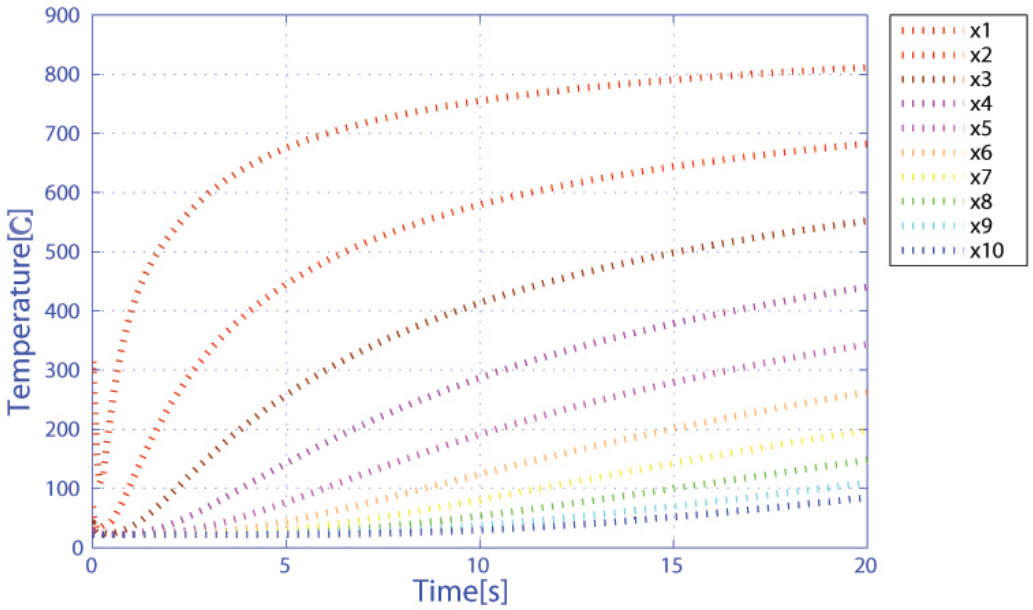

Figure 4.3: Temperature distribution in the radial direction of roll with varying depth

at the points x7, x8, x9 and x10, are negligible due to the thermal resistance of work roll material. So the heat transfer effect in the radial direction by conduction and radiation is significant only upto a depth of 30mm from the surface. The value of each nodal heat flux and temperature is used in the next phase of simulation.

4.2 Convection Model

The maximum heat transfer by the effect of convection to ambient air from roller surface is calculated from this simulation. The heat flux variation in z direction is plotted with different x coordinate values shown in Figure 4.4. From the figure the maximum heat flux of $2.104 \times 10^4 W/m^2$ is generated at the middle of the plate surface. Average heat flux is $1.5 \times 10^4 W/m^2$. For the next phase the value of average heat flux generated from this model is used combined.

4.3 Combined Heating Model

A coupled analysis of results from the previous model is performed in the phase to find the total heat distribution by heating effect of roller. As per the distribution of model in Section 3.3, the defined problem is viewed in two different approaches.

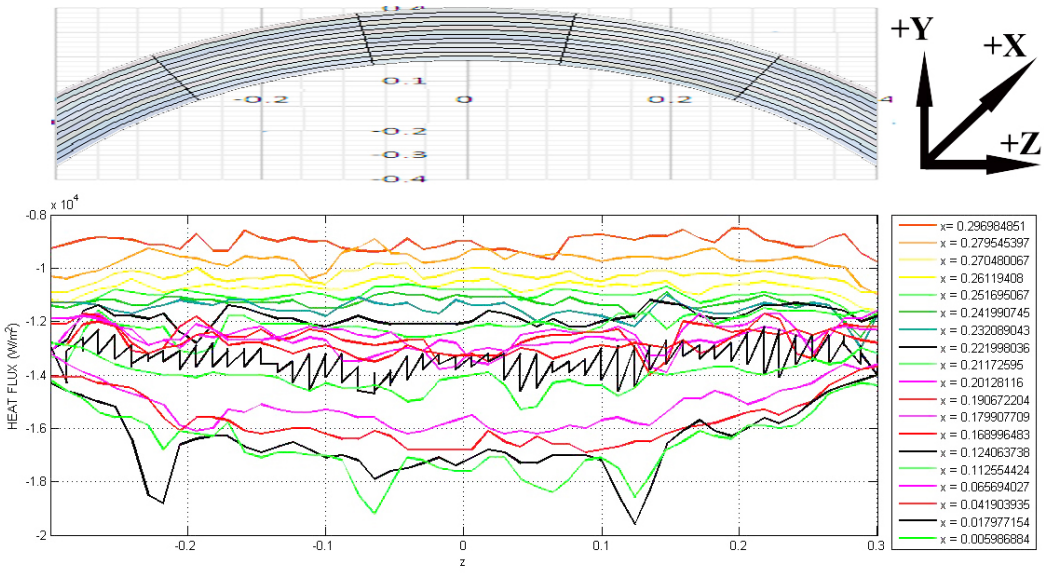

Figure 4.4: Convective heat flux distribution through varying nodal points of x direction with respect to width of barrel.

A comparative study of thermal quantities with varying diameter such as 850mm, 800mm and 750mm is performed here. It is concluded that there is no much difference I the performance with less variations in diameter. A comparative study of thermal quantities with varying roll speed like 200 rpm, 160 rpm 80 rpm, 50 rpm and 10 rpm is also performed. All the studies and simulations are done on the basis of steady state transient conditions. The result from each approach is summarized as follows.

Approach 1

In this approach the total part of the roller body is divided into 36 equal parts and the division is done for equal angular intervals in circular phase of the work roll. Thus each part of the roll is provided with different boundary conditions with respect to time. The circular phase of the work roll is considered as adiabatic. So the atmospheric heat transfer variation in this face is not affected. A heat flux of $1 \times 10^7 W/m^2$ is passed to each angular sector circumferential surface with respect to time. That is the heat flux at a particular angular sector at a particular time interval is passed to next sector in the next time interval. Similarly with the temperature of $910^0 C$. The temperature variation and heat flux in steady state

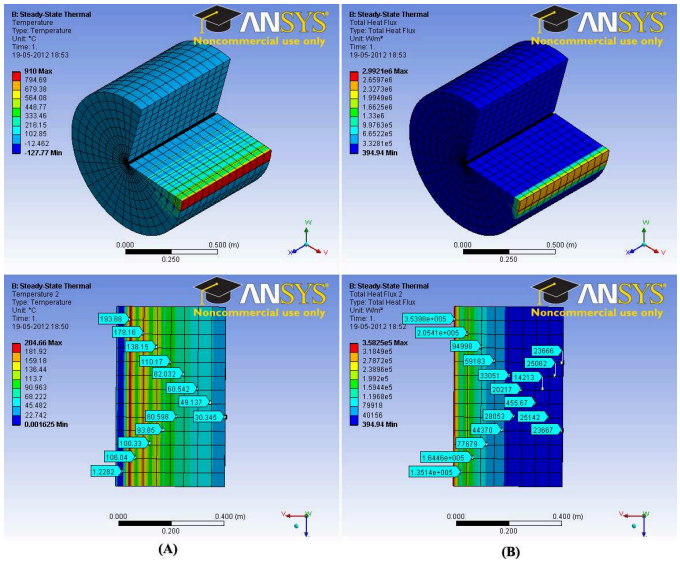

Figure 4.5: [a] Temperature Contour of Work Roll in Steady State Analysis [b] Heat Flux Contour of Work Roll in Steady State Analysis

analysis is shown in Figure 4.5. The figure shows the physical phenomena. The depth wise thermal distribution of steady state analysis is also shown in Figure 4.5. The minimum temperature is 30.345^0C. After a complete cycle of 5 revolutions, the temperature of the surface is 910^0C.

The same procedure is carried out for transient state also (Figure 4.6). Here, the maximum temperature is 980^0C. From both steady state and transient state analysis, the transient state analysis approaches practical scenario. The beginning of the simulation result is marked with a higher amount of temperature fluctuations at the surface while the core temperature of the work roll tends to increase gradually. The inner core responds slowly to the sudden changes to the sudden changes of temperature while the work roll comes in contact with the hot metal strip in the roll bite region. The depth wise temperature variation from the roll surface during hot rolling process is illustrated in Figure 4.7(b). The response of the inner core and outer surface is portrayed in the figure with varying depth from surface i.e. x1 is the outer surface and x2, x3, x4, x5 are 50 mm,100 mm,150 mm,200 mm respectively. From this graph the temperature variation in x4 and x5 is negligible. The maximum temperature occurring at the surface is 1050^0C. The maximum temperature at X2 is 450^0C. Time taken for 1 revolution is 1 second.

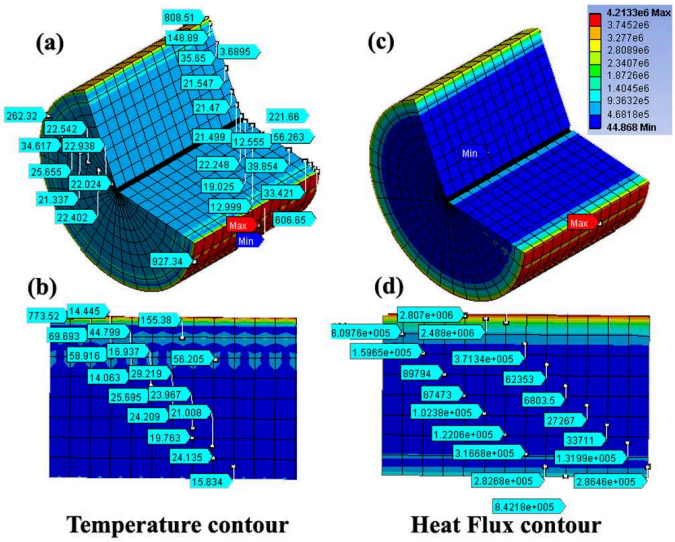

Figure 4.6: [a] and [b] Temperature Contour of Work Roll in Transient State Analysis [c] and [d] Heat Flux Contour of Work Roll in Transient State Analysis

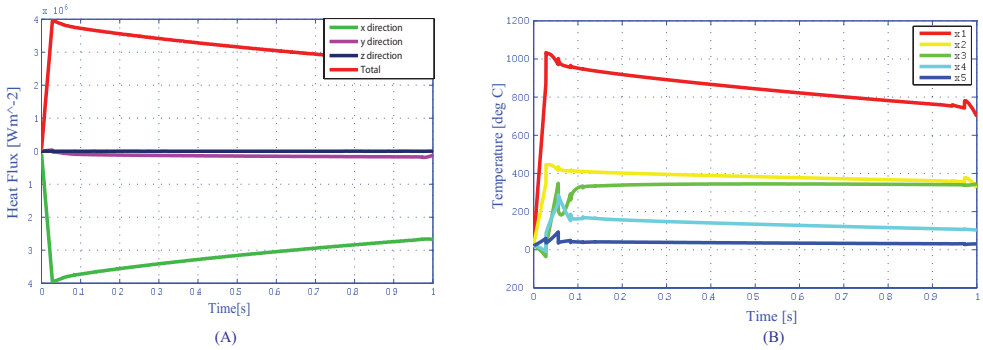

Figure 4.7: [a] Heat Flux Distribution of a key point on the Roll Surface [b] Depth Wise Temperature Variation from the roll surface

The heat flux variation of the surface in x, y, z direction is illustrated in Figure 4.7(a). The maximum heat flux is $4 \times 10^6 W/m^2$.

Approach 2

The methodology and analysis is performed here as per the model definition in Section 3.3. The boundary conditions and thermal parameters of Approach 1 are adopted here excluding angular division and heat source nature. Instead of moving heat source described in Approach 1, here, moving hot plates are the heat sources with a temperature of 1150^0C. The virtual plates are equivalent to metal strip thus providing a similar model to practical case. A constant heat flux of $1 \times 10^7 W/m^2$ is emitted from the surface of the virtual plates. By the effect of this

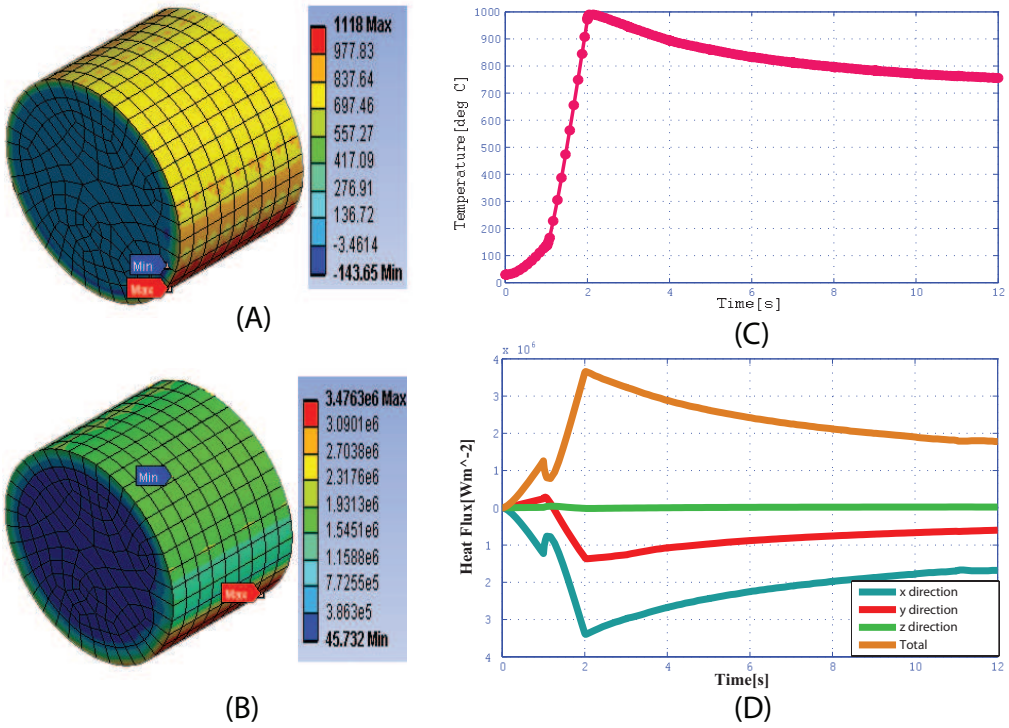

Figure 4.8: [a] Physical Representation of Temperature Contour [b] Physical Representation of Heat Flux Contour [c] Temperature Distribution of a key point on the roller surface with 5 rpm [d] Three Dimensional Heat Flux Distribution of a key point on the roller surface with 5 rpm

emission, the temperature field of the roller is varying to a maximum of 1050^0C. A time dependent thermal field variation with different rolling speed is performed here. Figure 4.8 illustrates the thermal profile performance with a rotating speed of 5 rpm. Physical representation of thermal quantities is shown in Figure 4.8(a) and Figure 4.8(b). The heat flux variation and temperature distribution of the surface of the roll are shown in Figure 4.8(c) and Figure 4.8(d) respectively from that graph.

Figure 4.9 shows the temperature and heat flux variation for three revolutions. From figure 4.9(a), the heat flux gradually reduces with each revolutions and Figure 4.9(b) shows that the surface temperature of roller increases with each revolution. This phenomenon is happened by the effect of heat accumulation. The temperature difference of roller strip reduces with each revolution since the heat transfer will also be reduced.

The same procedure of previous analysis is performed here with a rotating

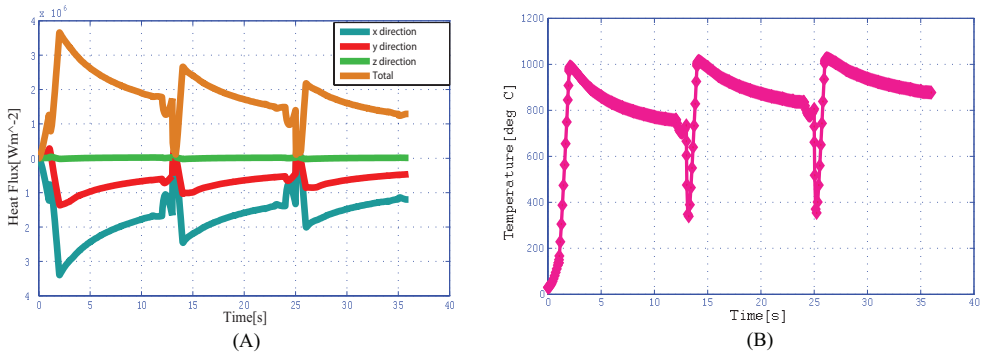

Figure 4.9: [a] Three Dimensional Heat Flux Distribution of a key point on the roller surface with 5 rpm for 3 revolutions [b] Temperature Distribution of a key point on the roller surface with 5 rpm for 3 revolutions

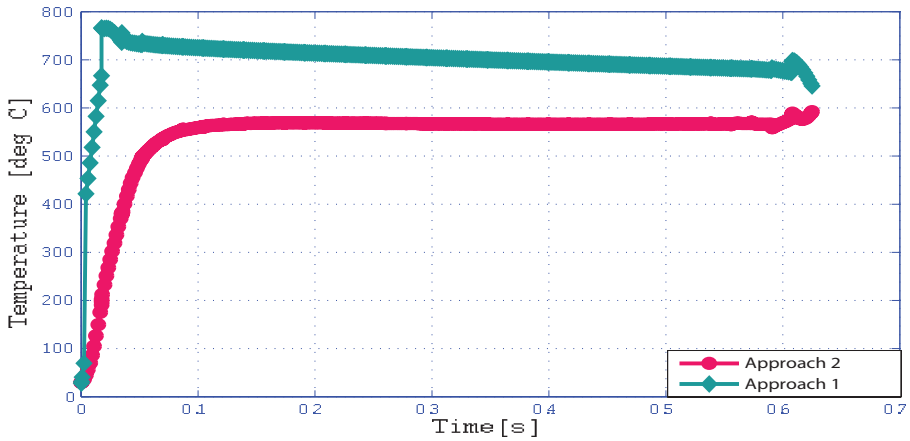

Figure 4.10: Temperature Distribution Comparison of Approach 1 and 2

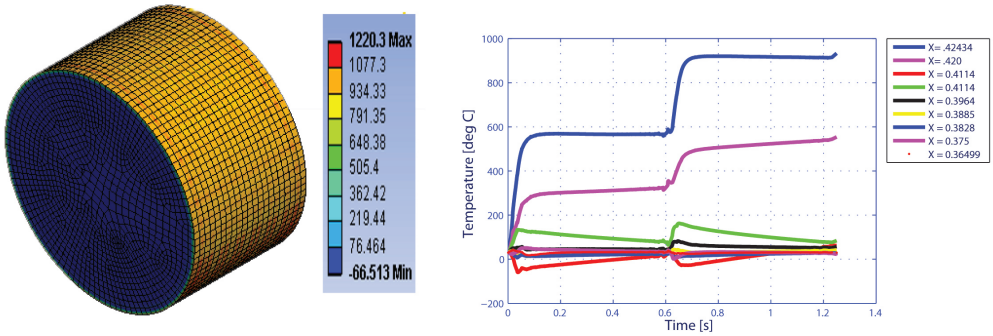

Figure 4.11: Temperature Variation in different layer of work roll for 2 revolutions

speed of 100 rpm is shown in Figure 4.10. The variation of temperature in radial direction is also plotted at different radial points i.e. x=0.4244, x=0.4200, x=0.4110, x=0.3964, x=0.3880, x=0.3820, x=0.3750, x=0.3650. The highlighted feature from the figure is the rapid increase in temperature at the surface, though because the time of contact between the strip and work roll is very short. Only the skin of the work roll is subjected to very high thermal radiance. After one complete revolution, the maximum temperature of the surface is occurring at 590^0C. But in the first stage of next revolutions, the temperature variation rapidly increases to 920^0C due to heat accumulation and the same phenomenon is repeated for inner layers also, as shown in Figure 4.11.

From the starting of this analysis, results are striking with the evaluated amount of temperature variation occurred at the surface while the core temperature of the roll tends to increase slowly. The interior core responds slowly to the rapid change of temperature while the work roll comes in contact with the strip in the roll bite region. These results leads to the conclusion that, in the high speed rolling process heat conduction rate are very slow. Among the two approaches, Approach 2 shows better performance than the other(Figure 4.10). Transient state analysis results show that they are similar to practical scenarios. These results are leads to the conclusion that, in the high speed rolling process heat conduction rate are very slow.

4.4 Forced Cooling Model

Water Jet Impingement

Analysis and simulation of water jet is simulated in third modeling. Jet impingement is one of the very efficient solutions of cooling hot bodies as it produces a very high heat transfer rate by forced convection. The effects of nozzle geometry, jet to target spacing, operating conditions etc. on flow and heat transfer have been studied numerically and validated with experimental results. Numerical analysis of multiple circular and conical water jet vertically impinging on a circular plate is performed with different flow arrangement. This study aims to recommend the most suitable model in predicting this type of flow through an investigation of the

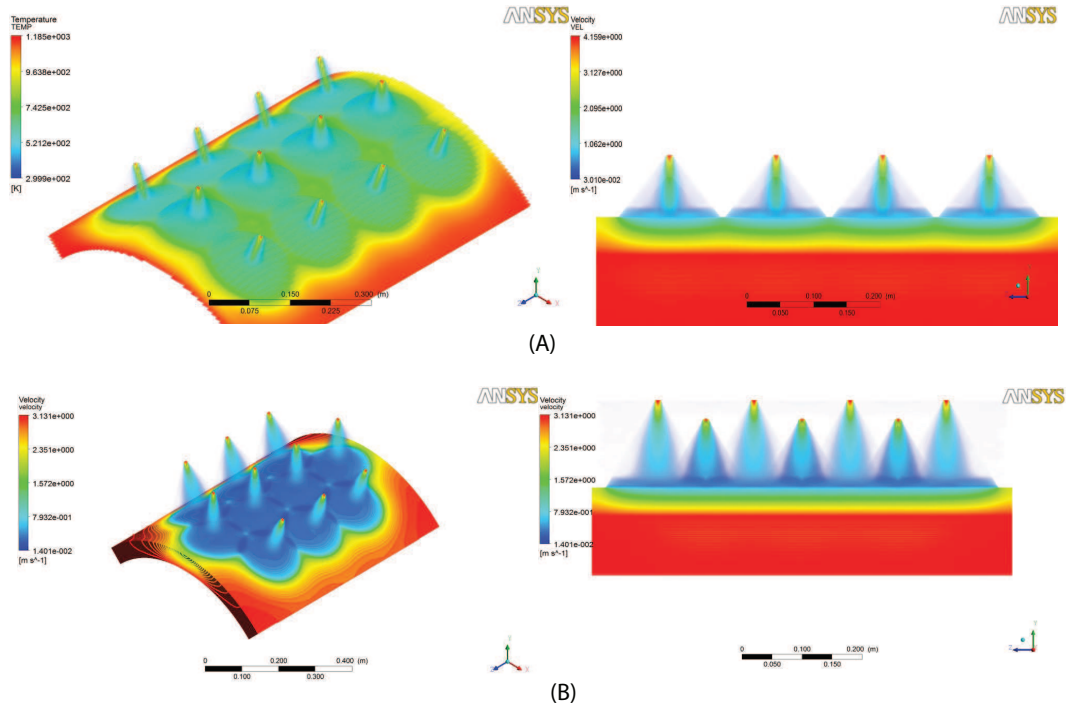

Figure 4.12: Physical and computational description of flow field and temperature contour of (a) linearly spaced nozzle arrangement (b) diagonally spaced nozzle arrangement

relative performance of $K\omega$ turbulence model (Shear-stress transport model) and find out the effect of heat transfer coefficient. Numerical calculations based on the CFD code AN SYS CFX 13 are conducted, the justification of the models are carried out by comparing the numerical results with existing experimental data. All the simulations are carried out with constant Reynoldss Number (30000). This model was used to observe the effect of controlled cooling sprays. For the purpose of the analysis it was assumed that the coefficients were applied to 10 percent of work roll surface and the rest of the surface to have a cooling arising from coolant wash over and air such that the average coefficient was $5000W/m^2K$. The heat input was taken to be $600KW/m$ width over the strip width. This simulation is carried out with different combinational and physical conditions such as:

- Circular Nozzle
  - Matrix array of 3x7 nozzles arrangements with different target to nozzle spacing (Figure 4.12(a))

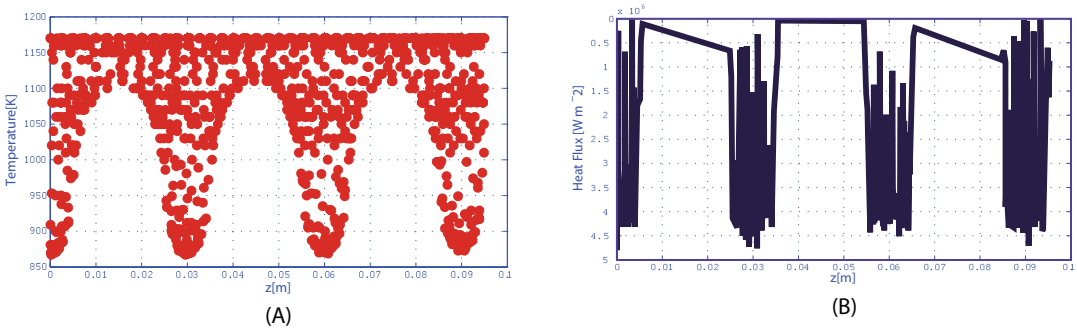

Figure 4.13: (a) temperature distribution of linearly spaced nozzle arrangement with respect to width of the roll barrel in jet roll interface region (b) Heat flux distribution of linearly spaced nozzle arrangement with respect to width of the roll barrel in jet roll interface region

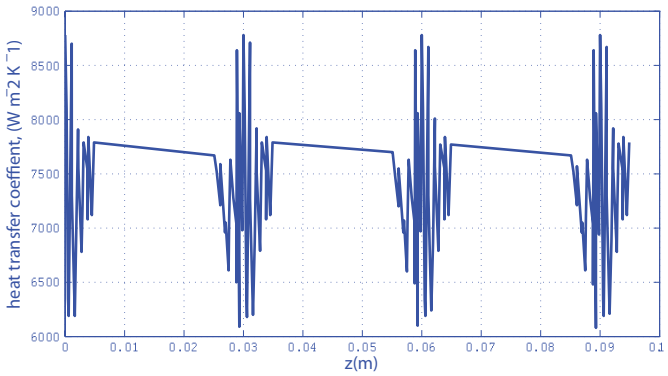

Figure 4.14: Heat transfer coefficient variation of linearly spaced nozzle arrangement with respect to width of the roll barrel in jet roll interface region

- Cone spray nozzle
  - Matrix array of 3x7 nozzles arrangements with different target to nozzle spacing and cone angle(Figure 4.12(b))
  - Array of 3x4 nozzles arrangements with diagonal spacing(Figure 4.12(c))

A matrix array of 3x7 circular nozzles arrangement with target to nozzle spacing of 30mm, 80mm, 150mm are carried out with this phase of study. Figure 4.13(a) and Figure 4.13(b) shows that the temperature and heat flux variation in axial direction of the roll surface. Since in a circular jet the impingement area is very less, the temperature variation is very less; the temperature variation of the roller surface is significant only in that area and the minimum temperature of roll surface is 850^0C. The maximum heat transfer is occurring in that area.

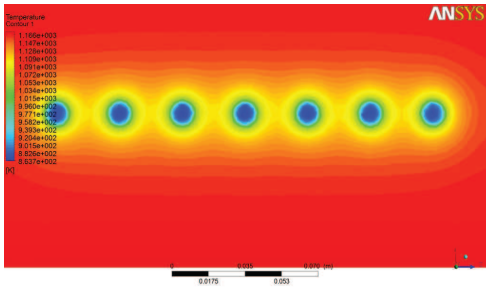

Figure 4.15: Temperature contour of roll surface after impinging of linearly spaced circular water jet

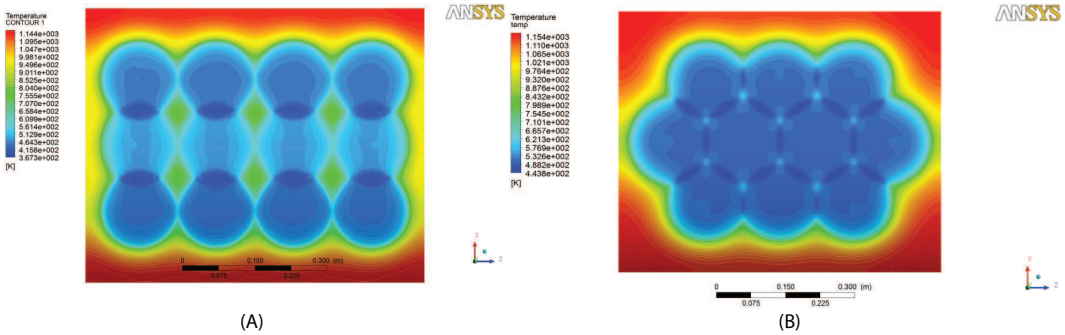

Figure 4.16: Temperature contour of roll surface after impinging of cone spray water jet by (a) linearly spaced nozzle arrangement (b) diagonally spaced nozzle arrangement

Figure 4.14 demonstrates heat transfer coefficient variation in axial direction of the impingement zone. The maximum heat transfer coefficient of $8750W/m^2K$ is occurring in the stagnation zone of the impingement area. Average heat transfer coefficient will be $7500W/m^2K$. The temperature contour of the target surface is shown in Figure 4.15. But the net effect of this nozzle arrangement results in less cooling efficiency. In order to increase this efficiency, the nozzle number should be increased by three times with very less nozzle to nozzle spacing. This arrangement increases the total impingement area in order to increase the cooling efficiency and reducing surface temperature.

In this thesis, cone spray nozzles of angle 600 are implemented rather than increasing the number of circular nozzles. Two types of arrangements are used. The temperature contour of target surface of the matrix array of nozzles and diagonal spacing arrangement are shown in Figure 4.16(a) and Figure 4.16(b) respectively. From these figures it is clear that arrangement 2 has more advantages such as more contact area and more cross-flow area than the other. Due to this

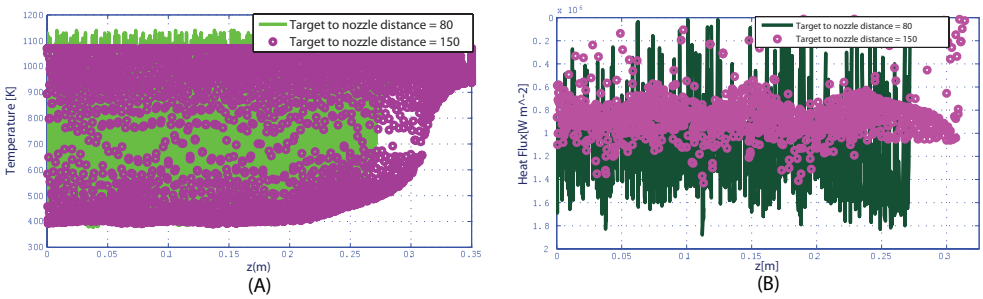

Figure 4.17: (a) Temperature variation on hot roll surface of jet- roller interface region after impinging of cone spray water jet with varying nozzle to target spacing (b) heat flux variation on hot roll surface of jet- roller interface region after impinging of cone spray water jet with varying nozzle to target spacing

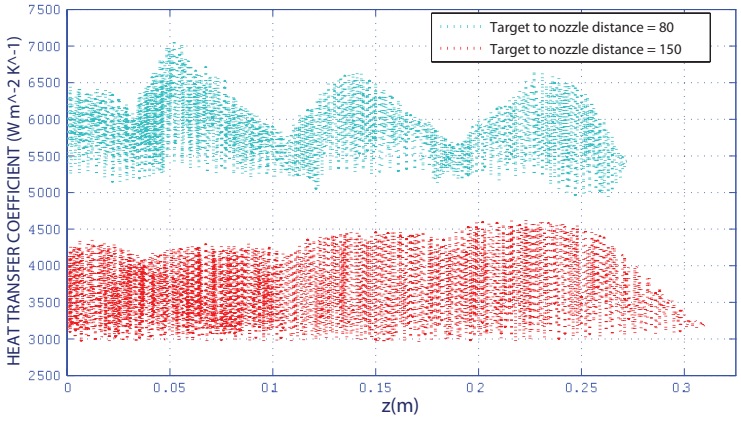

Figure 4.18: Heat transfer coefficient variation on hot roll surface of jet- roller interface region after impinging of cone spray water jet with varying nozzle to target spacing

cross flow more turbulence will happen in that area. This turbulence creation increases the overall heat transfer coefficient and heat flow. Figure 4.17(a) and Figure 4.17(b) illustrates the temperature variation and heat flow of different target to nozzle distances such as 80mm and 150mm. Maximum heat transfer occurs for 80mm target to nozzle distance and this also keeps minimum surface temperature. Heat transfer coefficient distributions of these two are plotted in Figure 4.18. From the figure, the maximum heat transfer of $7000W/m^2K$ occurs for 80mm target to nozzle distance. From this it is concluded that heat transfer will be increasing with decrease in nozzle to target space. The average heat transfer coefficient increases with increase in Reynoldss Number. At higher Reynoldss Number turbulence level increases and along with this, spread of the jet also

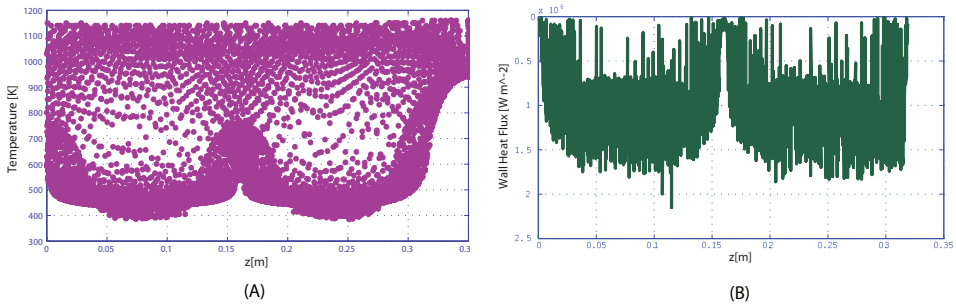

Figure 4.19: (a) Temperature variation on hot roll surface of jet- roller interface region after impinging of cone spray linearly spaced water jet (b) heat flux variation on hot roll surface of jet- roller interface region after impinging of cone spray linearly spaced water jet

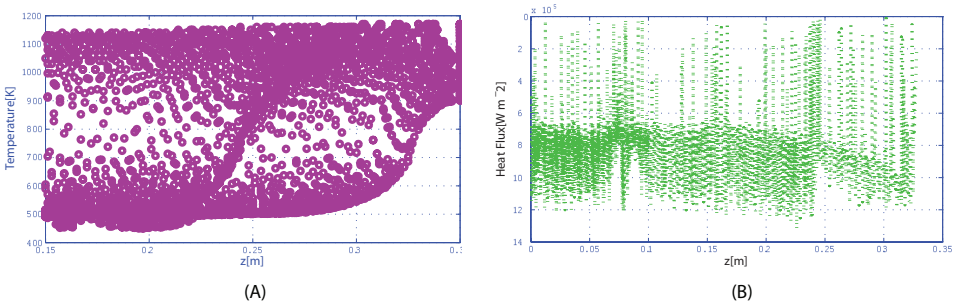

Figure 4.20: (a) Temperature variation on hot roll surface of jet- roller interface region after impinging of cone spray diagonally spaced water jet (b) Heat flux variation on hot roll surface of jet- roller interface region after impinging of cone spray diagonally spaced water jet

increases. The net amount of fluid that comes out of the jet is also higher for higher Reynoldss Number which causes better heat transfer performance.

Figure 4.19 shows the temperature and heat flux variation of matrix array of 3x4 nozzle arrangement with a target to nozzle spacing of 80mm. Figure 4.20 shows temperature and heat flux variation of array of 3x4 nozzle arrangement with diagonal spacing 150mm. The heat transfer coefficient distribution of both arrangements is shown in Figure 4.21. From this study, diagonal spacing (of 60mm) nozzle system with spacing of 80mm between nozzle and target has been evaluated as the optimised one. The heat transfer coefficient of this model is plotted in Figure 4.22. Seven number of nozzles are arranged in 3 rows in this model with a Reynoldss Number of 30000 and Nusselt Number ranging from 50 to 70. The value of heat loss from the target plate is estimated and is used for final simulation.

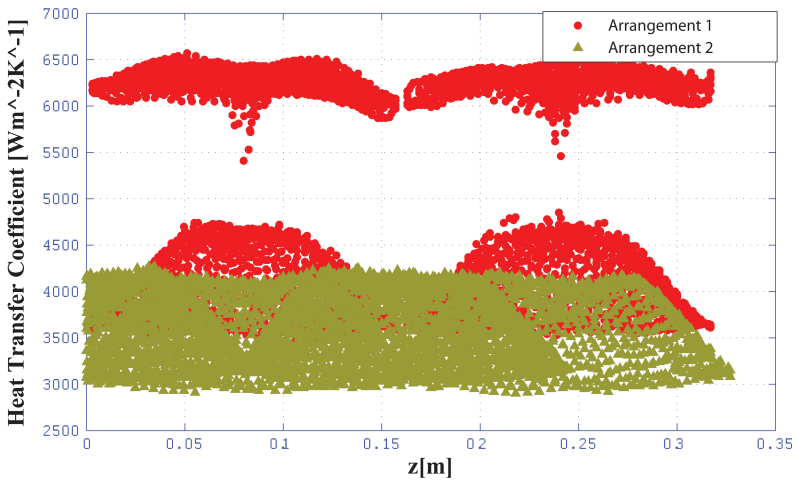

Figure 4.21: Comparison of heat transfer coefficient in different nozzle arrangement

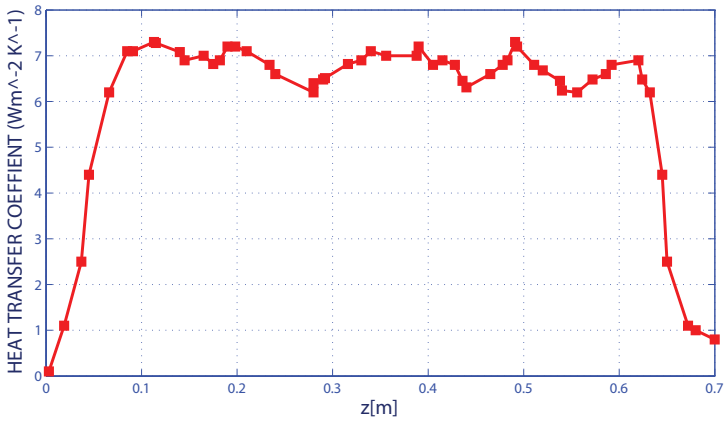

Figure 4.22: Variation of heat transfer coefficient with respect to width of the roll barrel in jet roll interface region of optimized model

4.5 Combined heating and cooling model

In the beginning of the rolling process the work roll temperature was assumed to be uniform room temperature (27^0C). The thermal condition of finishing stand hot rolling was taken as an example for calculation. Heat conduction and radiation heat transfer is only considered in this heating model. From the analysis the maximum surface temperature is occurring at work roll is 910^0C and it was a slow heating process. For the simplicity of simulation, work roll is considered as hollow cylinder with thickness 100mm and its both flat faces are kept as adiabatic. The angular variation of heat flow and temperature also consider in this

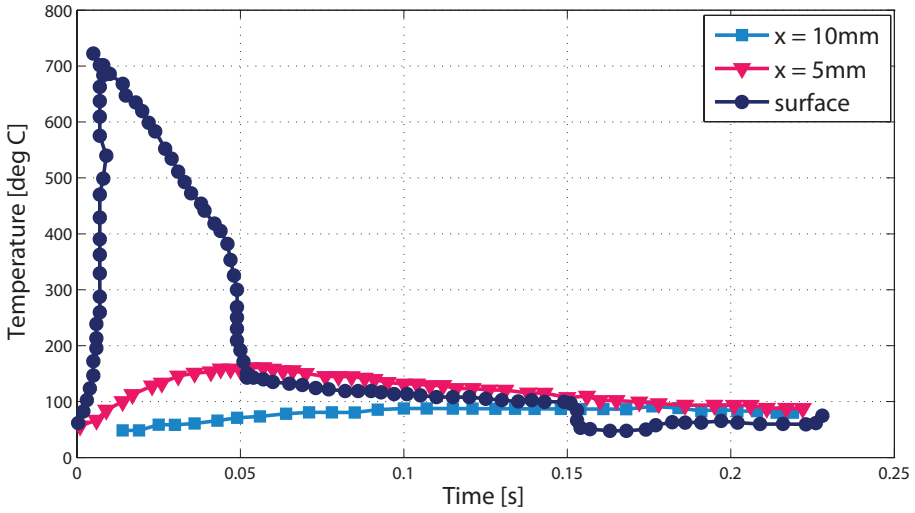

Figure 4.23: Temperature variation in different layer of work roll by the effect of optimized nozzle impact sprays in entrance and exit side of stand

analysis. From these results it can conclude that the temperature effect and heat flow variation will be significant only in the nearest layer of the surface of roll. Radiation effect is irrelevant after 30^0 angular nodal variation from conduction zone in both directions. All these heating and cooling models are combined to do the last step of simulation. The surface temperature of the roll is decreased to 32^0C after finishing rolling. Thereafter, the surface temperature of the work rolls experience the same cyclic variation along with the rolling of the successive steel slab. Temperature profile of the roll as predicted by the last simulation with all consideration at different nodal positions from the surface of roll is plotted in Figure 4.23. The predicted temperature variation at different depths from the roll surface have also been depicted in the figure. The region AB is the conduction and radiation heat transfer zone. BC, DE and FG are the convective heat transfer zone from roll surface to air. CD and EF are the water jet cooling region. To assess the accuracy of the model, it was employed to reproduce the conditions published by stevens[44] for a roughing mill operation. Stevens instrumented a work roll with thermocouple and measured the temperature response at different depths below the surface. With the operating conditions for the roughing mill work roll described in that paper, the work roll temperature variation was predicted with the present model. The result for the first 4 successive revolutions is plotted in Figure

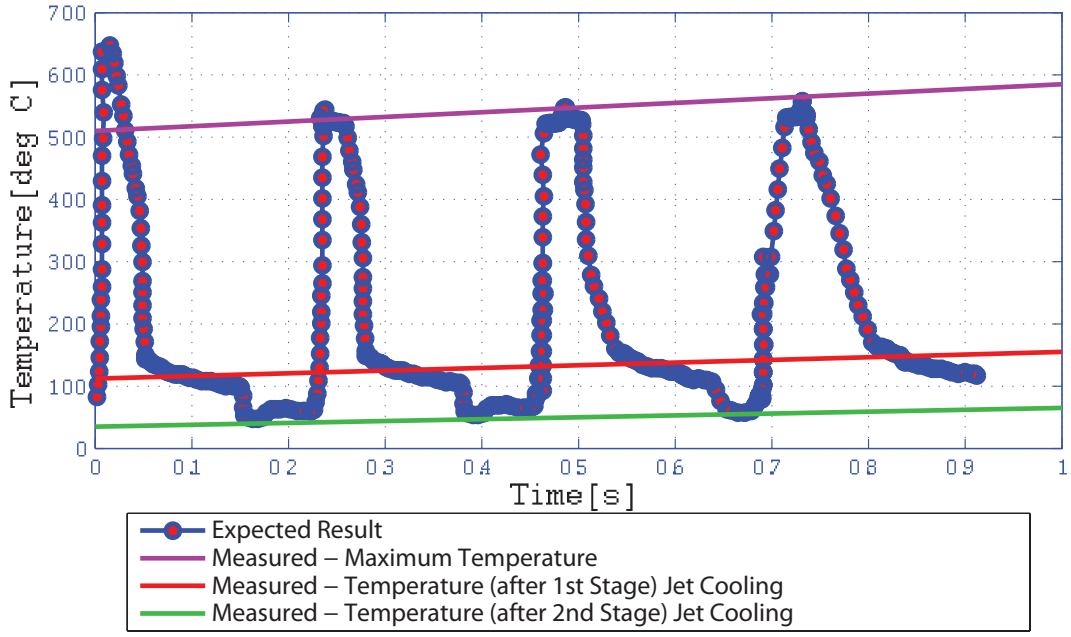

Figure 4.24: Surface Temperature variation of work roll by the effect of optimized nozzle impact sprays in entrance and exit side of stand for 4 successive revolution and validation with existing data

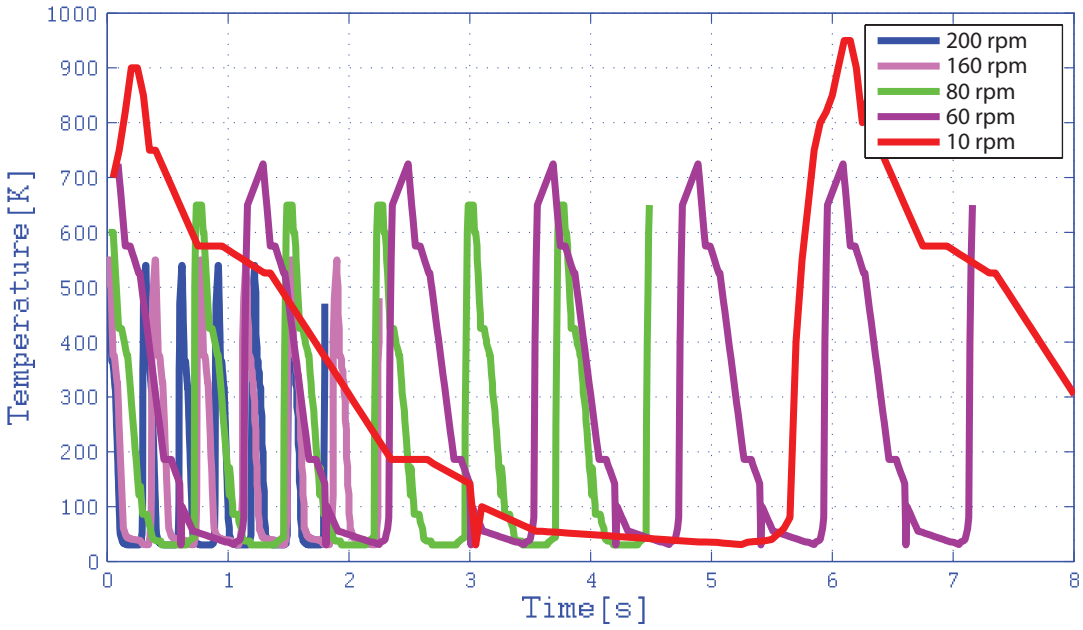

Figure 4.25: Variation of temperature field with respect to rotation speed of work roll

4.24. A comparison of the values predicted by the present model with stevens data is illustrated in this figure, which indicates fair agreement between predicted and measured values. The temperature variation of roll surface with respect to roll speed is illustrated in Figure 4.25. It leads that higher angular velocity of the work roll, minimize the roll surface temperature. Maximum temperature is occurring in 10 rpm and it gradually decreased with increasing roll speed. Work roll speed, nozzle geometry, computational characteristic of nozzle flow, work roll diameter and working environment are playing important role in hot rolling process.

5 Concluding remarks

5.1 Conclusion

From this project work, the following conclusions are made

- The temperature profile of an random cross section of work roll were calculated during the hot rolling process and the period of rolling process using 3 dimensional finite element method, and the model of variation of the roll surface temperature was analysed.
- Cyclic nature of Work Roll surface temperature variation is analysed.
- The increase of convective heat transfer coefficient at roll-strip interface region minimizes the temperature of the roll surface.
- Temperature effect and heat flow variation will be significant only in the nearest layer of the surface of roll.
- The increase of convective heat transfer coefficient at forced water jet cooling interface increases the cooling efficiency.
- Increases the area of contact in fluid solid interface in water jet region reduces the net temperature of the work roll surfaces.
- Cone spry water jet model gets the better result than circular nozzle arrangement.
- Closely packed jet arrangement (diagonal spaced model) gets the better result than normal spaced nozzle arrangement.

- Higher angular velocity of the work roll leads to minimize the roll surface temperature.
- The response of the roll to cooling change is a complex function of time, being rapid at first but becoming very slow as the cooling changes penetrate deeper in to the roll.

5.2 Scope of Future Work

- Numerical results with experimental validation.
- Optimization of different parameters to reduce the thermal fatigue
- Optimization of different parameters to reduce the thermal expansion
- Optimization of water jet impingement heat transfer effect for getting maximum cooling efficiency and roll life.

References

[1] Martha P. Guerrero, Carlos R. Flores, Antonino Perez, Rafael Colas,"Modeling heat transfer in hot rolling work rolls," *Journal of Materials Processing Technology*, vol. 94, pp. 52-59, 1999.

[2] F.D. Fischer, W.E. Schreiner, E.A. Werner and C.G. Sund.,"The temperature and stress fields developing in rolls during hot rolling," *Journal of Materials Processing Technology*, vol. 150, pp. 263-269, 2004.

[3] C. H. HUANG and T. M. JU.,"The estimation of surface thermal behavior of the working roll in hot rolling processes," *International Journal Heat Mass Transfer*, vol. 38, Issue. 6, pp. 1019 - 1031, 1995.

[4] O. M. Alifanov,"Solution of an inverse problem of heat conduction by iteration methods," *Journal of Engineering and Physics*, vol. 26, Issue. 4, pp. 471-476, 1974.

[5] C. H. Huang and M. N. Ozisik,"Inverse problem of determining unknown wall heat flux in laminar flow through a parallel plate duct," *Numerical Heat Transfer*, A 21, pp. 55-70, 1992.

[6] C. H. Huang and M. N. Ozisik,"Inverse problem of determining the unknown strength of an internal plate heat source," *Journal of Franklin Inst.*, vol. 329, pp. 751-764, 1992.

[7] C. H. Huang and M. N. Ozisik,"Conjugate gradient Surface thermal behavior 1031 method for determining unknown contact conductance during metal casting," *Int. J. Heat Mass Transfer*, vol. 35, pp. 1779-1786, 1992.

[8] Y.T. Azene , R. Roy , D. Farrugia, C. Onisa , J. Mehnen and H. Trautmann.,"Work roll cooling system design optimisation in presence of uncer-

tainty and constrains," *CIRP Journal of Manufacturing Science and Technology*, vol. 2, pp. 290-298, 2010.

[9] M raudensky, J Horsky and M Pohanka.,"Optimal cooling of rolls in hot rolling," *Journal of material processing technology*, vol. 125 - 126, pp. 700 - 705, 2002.

[10] Mohamed Hamraoui.,"Thermal behavior of rollers during the rolling processes," *Journal of Applied Thermal Engineering*, vol. 29, pp. 2386-2390, 2009.

[11] Mohammad Abbaspour and Ahmad Saboonchi.,"Work rolls thermal expansion control in hot strip mill," *Journal of Applied Mathematical Modeling*, vol. 32, pp. 26522669, 2008.

[12] Pao Tung Hsu, Yue Tzu Yang and Chao-Kuang,"A Three-Dimensional Inverse Problem of Estimating the Surface Thermal Behavior of the Working Roll in Rolling Process," *Journal of manufacturing science and engineering*, vol. 122, pp. 76-82, 2000.

[13] S. Serajzadeh.,"Effects of rolling parameters on work-roll temperature distribution in the hot rolling of steels," *International journal of advanced manufacturing technology*, vol. 35, pp. 859866 , 2008.

[14] Serajzadeh S, Taheri A.K and Mucciardi, F."Unsteady state work roll temperature distribution during continuous hot slab rolling," *International journal of Mechanical Sciences*, vol. 44, pp. 24472462, 2002.

[15] Arif A.F.M, Khan O and Zubair S.M.,"Prediction of roll temperature with a non-uniform heat flux at tool and work piece interface," *Heat and Mass Transfer*, vol. 41, Issue.1, pp. 7594, 2004.

[16] Khan O, Jamal A, Arshed G, Arif A and Zubair S.,"Thermal analysis of a cold rolling process - A numerical approach," *Numerical Heat Transfer Part A: Applications*, vol. 46, Issue. 6, pp. 613635, 2004.

[17] Ye, X and Samarasekera,"The role of spray cooling on thermal behavior and crown development in hot strip mills work rolls," *Iron and Steelmaker*, vol. 21, pp. 4960, 1994.

[18] Sun C.G, Yun C.S, Chung J.S and Hwang S.M.,"Investigation of thermo mechanical behavior of a work roll and of roll life in hot strip rolling," *Metall. Mat. Transaction*, A 29, pp. 24072424, 1998.

[19] Prez A, Corral R.L Fuentes and R Colas R.,"Computer simulation of the thermal behavior of a work roll during hot rolling of steel strip," *Journal of Materials Processing Technology*, vol. 153, pp. 894899, 2004.

[20] Corral R.L, Cols R and Prez A.,"Modeling the thermal and thermo-elastic responses of work rolls used for hot rolling steel strip," *Journal of Materials Processing Technology*, vol. 154, pp. 886893, 2004.

[21] Peretic M.J, Seldel J and Kramer S.,"Coordinated application of roll gap lubrication, work roll cooling and anti peeling systems in hot rolling mills," *Iron and Steel Technology*, vol. 1, Issue. 5, pp. 2736, 2004.

[22] Sikdar S, and John S.,"Simulation of thermal history of work roll of finishing stands in a hot strip milla numerical approach," *Iron making and Steelmaking*, vol. 33, Issue. 6, pp. 493499, 2006.

[23] Rahman M.M, Dontaraju P, and Ponnappan R,"Confined jet impingement thermal management using liquid ammonia as the working fluid," *In: Proceedings of ASME IMECE*, pp. 17-22, November 2002.

[24] Stevens J, and Webb B.W,"Local heat transfer coefficients under an axisymmetric, single-phase liquid jet," *Heat Transfer in Electronics*, vol. 111, pp. 113119, 1989.

[25] Garimella S.V, and Rice R.A,,"Confined and submerged liquid jet impingement heat transfer," *Journal of Heat Transfer*, vol. 117, pp. 871-877, 1995.

[26] Gomi T, and Webb B.W,"Local characteristics of impingement heat transfer with oblique round free-surface jets of large prandtl number liquid," *International Journal of Heat and Mass Transfer*, vol. 40, Issue. 10, pp. 2249-2259, 1997.

[27] Lee D.H, Chung Y.S, and Kim D.S,"Turbulent flow and heat transfer measurements on a curved surface with a fully developed round impinging jet," *International Journal of Heat and Fluid Flow*, vol. 18, pp. 160-169, 1997.

[28] Kornblum Y, Goldstein R.J,"Jet impingement on semi-cylindrical concave and convex surfaces: part II - heat transfer," *International Symposium on Physics of Heat Transfer in Boiling and Condensation*, pp. 597-602, 1997.

[29] Lee D.H, Chung Y.S, and Kim M.G,"Turbulent heat transfer from a convex hemispherical surface to a round impinging jet," *International Journal of Heat and Mass Transfer*, vol. 42, pp. 1147-1156, 1999.

[30] Tong A.Y,"A numerical study on the hydrodynamics and heat transfer of a circular liquid jet impinging onto a substrate," *Numerical Heat Transfer*, vol. 442, pp. 1-9, 2003.

[31] Cornaro C, Fleischer A.S, and Goldstein R.J,"Flow visualization of a round jet impinging on cylindrical surfaces," *Experimental Thermal and Fluid Science*, vol. 20, pp. 66-78, 1999.

[32] Cornaro C, Fleischer A.S, Rounds M, and Goldstein R.J,"Jet impingement cooling of a convex semi-cylindrical surface," *Journal of Thermal Science*, vol. 40, pp. 890-898, 1999.

[33] Fleischer A.S, Kramer K, and Goldstein R.J,"Dynamics of the vortex structure of a jet impinging on a convex surface," *Experimental Thermal and Fluid Science*, vol. 24, pp. 169-175, 1999.

[34] Baonga J. B, Louahlia-Gualous H, and Imbert M,"Experimental study of the hydrodynamic and heat transfer of free liquid jet impinging a flat circular heated disk," *Applied Thermal Engineering*, vol. 26, pp. 1125- 1138, 2006.

[35] Inada S, Miyasaka Y, and Izumi R,"A study on the laminar-flow heat transfer between a two-dimensional water jet and a flat surface with constant heat flux," *n: Bulletin of the JSME*, vol. 24, , 1982.

[36] Carper H.J, Jr,"Impingement cooling by liquid jet," *In: Heat Transfer Division 1989 ASME HTD*, vol. 117, 1998.

[37] Liu X, and Lienhard V,"Liquid jet impingement heat transfer on a uniform flux surface," *In: Heat Transfer Phenomena in Radiation, Combustion and Fires1989 ASME HTD*, vol. 106, 1989.

[38] Wadsworth D.C, and Mudawar I,"Cooling of a multichip electronic module by means of confined two-dimensional jets of dielectric liquid," *Heat Transfer in Electronics*, vol. 111, pp. 79-87, 1989.

[39] Gau C, and Chung C.M,"PSurface curvature effect on slot-air-jet impingement cooling flow and heat transfer process," *Journal of Heat Transfer*, vol. 113, pp. 858-864, 1991.

[40] Stevens J, and Webb B.W,"Measurements of the free surface flow structure under an impinging, free liquid jet," *Journal of Heat Transfer*, vol. 114, pp. 79-84, 1992.

[41] Martin, H.,"Heat and mass transfer between impinging gas jets and solid surfaces," *Advanced Heat Transfer*, vol. 13, pp. 1-60, 1977.

[42] N. ZUCKERMAN and N. LIOR.,"Jet Impingement Heat Transfer- Physics, Correlations, and Numerical Modelling," *ADVANCES IN HEAT TRANSFER*, vol. 39, pp. 565-631, 2006.

[43] Viskanta, R.,"Heat transfer to impinging isothermal gas and flame jets," *Exp. Thermal Fluid Science*, vol. 6, pp. 111-134, 1993.

[44] PG Stevens, KP Ivens and P Harper ,"Increasing work roll life by improved roll cooling practice," *Journal of the Iron and Steel Institute*, pp. 1-11, 1971.